

An Evaluation of Grain Boundary Engineering Technology and Processing  
Scale-up

by

Jeffrey A. Zelinski

B.S., Mechanical Engineering  
University of Michigan, 2003

Submitted to the department of Materials Science and Engineering in partial fulfillment  
of the requirements for the degree of

Master of Engineering in Materials Science and Engineering

at the

Massachusetts Institute of Technology

September 2005

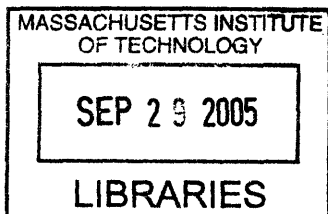
© 2005 Jeffrey A Zelinski. All rights reserved.

The author hereby grants to MIT permission to reproduce and to  
distribute publicly paper and electronic copies of this thesis document in whole or in part.

Signature of Author: \_\_\_\_\_  
Department of Materials Science and Engineering  
August 11, 2005

Certified by: \_\_\_\_\_  
Christopher A. Schuh  
Danae and Vasilios Salapatas Associate Professor of Metallurgy  
Thesis Supervisor

Accepted by: \_\_\_\_\_  
Gerbrand Ceder  
R.P. Simmons Professor of Materials Science and Engineering  
Chair, Departmental Committee on Graduate Students



ARCHIVES



# An Evaluation of Grain Boundary Engineering Technology and Processing Scale-up

by

Jeffrey Zelinski

Submitted to the department of Materials Science and Engineering on August 11, 2005 in  
Partial Fulfillment of the Requirements for the degree of Master of Engineering in  
Materials Science and Engineering.

## **Abstract**

Grain boundary engineering is the manipulation of low stacking-fault energy, face-centered cubic material microstructures to break the connectivity of the general grain boundary network through the addition of special grain boundaries. Grain boundary engineering processing consists of thermomechanical cycling, i.e. repeated strain and annealing sequences and provides a method of producing more robust polycrystalline materials. This evaluation presents an introduction to the fundamental principles of grain boundary engineering, reviews the processing techniques and relevant intellectual property, analyzes the processing variables and their effect on a manufacturing line, surveys the current market and competition, and provides a preliminary cost analysis.

Thesis Supervisor: Christopher A. Schuh

Title: Danae and Vasilios Salapatas Associate Professor of Metallurgy



## **Acknowledgements**

I would like to thank my fellow students in the M.Eng program. It was a great year and I'm fortunate to have been able to share it with everyone. I would like to thank Megan Frary who was so welcoming from the first time I visited MIT as a prospective and provided all the assistance I could ask for while being introduced to grain boundary engineering. I would also like to thank the rest of the Schuh group for offering a fun and social atmosphere during my short stay. Finally, I'd like to thank Chris Schuh for providing me with this wonderful topic to study while completing the Master of Engineering program.



## Table of Contents

<b>Abstract</b> .....	<b>3</b>
<b>Acknowledgements</b> .....	<b>5</b>
<b>1. Grain Boundary Engineering Fundamental Principles</b> .....	<b>8</b>
1.1 <i>Introduction</i> .....	8
1.2 <i>Grain Boundaries</i> .....	8
1.3 <i>Grain Boundary Affected Material Properties</i> .....	10
1.3.1 Solute Segregation and Corrosion .....	10
1.3.2 Intergranular Cracking.....	12
1.3.3 Creep.....	13
1.4 <i>Grain Boundary Connectivity</i> .....	13
1.5 <i>Grain Boundary Engineering Effectiveness</i> .....	14
<b>2. Processing and Manufacture</b> .....	<b>18</b>
2.1 <i>Introduction</i> .....	18
2.1.1 Strain Annealing .....	18
2.1.2 Strain Recrystallization.....	20
2.2 <i>Intellectual Property (IP) Review</i> .....	22
2.2.1 Grain Boundary Engineering IP.....	22
2.2.1.1 United States Patent #5,817,193 .....	23
2.2.1.2 Japan Patent JP2003253401.....	24
2.2.1.3 United States Patent Application Pub. No. US 2004/0156738 A1 .....	24
2.2.1.4 United States Patent #6,129,795 .....	25
2.2.1.5 United States Patent #6,344,097 .....	26
2.2.2 Intellectual Property Strategy .....	26
2.3 <i>Processing Analysis</i> .....	28
2.3.1 Benchmark Processing Conditions .....	29
2.3.2 Individual Cycle Analysis.....	30
2.3.3 Individual Variable Analysis .....	33
2.3.4 Strain Annealing Analysis .....	36
<b>3. Market Analysis, Competition, and Cost Analysis</b> .....	<b>38</b>
3.1 <i>Market Analysis</i> .....	38
3.2 <i>Competition</i> .....	41
3.3 <i>Cost Analysis</i> .....	42
<b>Conclusions</b> .....	<b>49</b>
<b>References</b> .....	<b>50</b>
<b>Appendix A: Derivation of Rolling Process Equations</b> .....	<b>54</b>
<b>Appendix B: Derivation of Annealing Process Equations</b> .....	<b>63</b>
<b>Appendix C: Derivation of Cooling Process Equations</b> .....	<b>72</b>

# 1. Grain Boundary Engineering Fundamental Principles

## 1.1 Introduction

The concept of grain boundary design and control was first proposed nearly 20 years ago by Watanabe [1] and has since come to be called “grain boundary engineering”. Grain boundary engineering focuses on the fact that bulk properties of polycrystalline materials are controlled not only by the size of the grains, but also by the grain boundary character distribution (GBCD) and further, by the connectivity of the material’s grain boundaries [20, 25, 78-79]. Since grain boundaries are known to have an affect on nearly all material properties [7], grain boundary engineering aims to invoke some control over their effects by enhancing their resistance to degradations [86]. Even beyond this, the large variety of possible orientations and interactions of grain boundaries mean that encounters between neighboring grains can produce properties unachievable in single-crystal materials providing for new polycrystalline materials with higher performance and versatility than ever before [2]. In many cases, grain boundary engineering a material simply consists of tailoring the manufacturing process with specific idealized parameters (such as deformation amount or annealing time and temperature) that generate superlative grain boundary orientations more resistant to degradations [11-12, 14-15, 21-22, 32]. This enhanced polycrystalline material, or as it will be referred to from now on, grain boundary engineered material, endeavors to improve many engineering materials already in wide use and drive us into the high performance age of the 21<sup>st</sup> century.

## 1.2 Grain Boundaries

Grain boundaries in polycrystalline materials can be viewed as nonequilibrium defects in atomic arrangements arising from the misorientation of crystal lattices in adjacent grains with identical chemical composition and crystallography. In the transition between two misoriented crystal lattices, the bonds between the atoms differ from those of the regular crystal lattice. This difference in bond energy gives the grain boundaries different properties than the bulk crystals they separate. Thus, the three-dimensional grain boundary network throughout a material creates a linked material structure with properties that can contribute substantially to the overall behavior of the material,

especially when the properties of grain boundaries are typically worse than those of the bulk crystal.

The rise in grain boundary engineering research and its emergence as a promising technology can be attributed largely to the proliferation of electron backscatter diffraction (EBSD) technology [77]. EBSD is a scanning electron microscope (SEM) based technique that works by positioning a stationary beam of electrons on a specimen's surface and relating the resulting diffraction pattern back to its original position on the specimen to obtain crystallographic orientation information [4, 77]. In this way, grain misorientations can be rapidly measured and classified as either special or general. EBSD results and data can be output in either statistical or pictorial formats such as the image of a copper microstructure shown next to its corresponding SEM image in Figures 1 and 2.



**Figure 1. Scanning electron microscope image of copper showing grains and grain boundaries [3].**

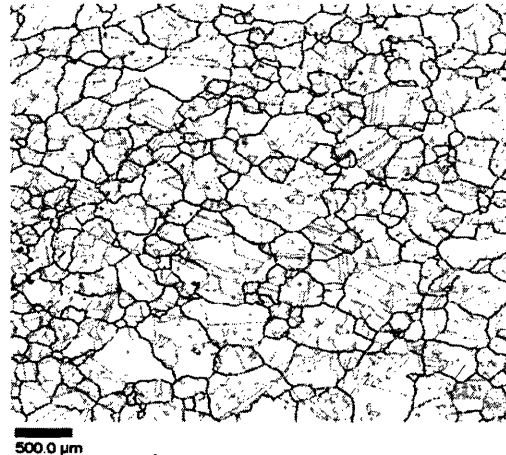


**Figure 2. Electron backscatter diffraction image showing grain boundaries classified as special (green) or general (red) [3].**

As mentioned above, a binary classification of either special or general can be assigned to grain boundaries during EBSD. Binary classification is necessary because grain boundaries have five macroscopic degrees of freedom [85] and correlation to material properties becomes difficult to manage when considering all five. Therefore, a categorization of either special or general allows for much easier correlation of the GBCD to material property enhancements. The classification of special requires a

coincidence site lattice (CSL) value,  $\Sigma$ , of less than 29 [7] where this  $\Sigma$ -value is based upon the reciprocal density of coincident atomic lattice sites between two grains assuming interpenetration with one another (see Figure 3). A low  $\Sigma$ -value indicates a high degree of coincidence between grains and thus a better fit, lower interfacial energy and less free volume in the grain boundary. Since exact CSL

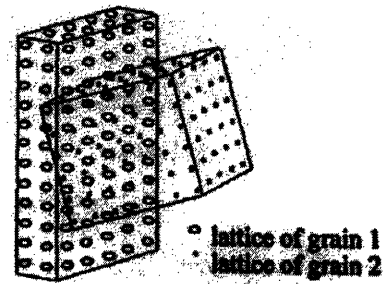


**Figure 3. Interpenetration of disoriented grains resulting in a small number of coinciding sites [4].**

misorientations are unusual, a grain boundary's measured misorientation angle is allowed to deviate from the ideal CSL angle by maximum angle,  $\Theta$ , which is commonly calculated using Brandon's criterion [5] or the more restrictive Palumbo-Aust criterion [6].

### 1.3 Grain Boundary Affected Material Properties

The binary classification of grain boundaries as either special or general has been developed and demonstrated by numerous studies throughout the last several years. Palumbo and Aust [7] include solute segregation, energy, diffusion, mobility, sliding, fracture, cavitation, hardening, resistivity, and corrosion as properties showing improvement at special boundaries. Although improvements in each of these properties could be useful, this evaluation will focus on property enhancements preventing solute segregation (sensitization), corrosion, cracking, and creep. Sensitization, corrosion, and cracking actually have many interrelating factors, however, each will have a few studies that focus on understanding their nature separately summarized in the following sections.

#### *1.3.1 Solute Segregation and Corrosion*

Grain boundaries possess different energetic states than the rest of the bulk crystal and can reduce this excess energy through interaction with lattice defects [88]. These include impurities or solute atoms that segregate to the grain boundaries creating a chemically different material as compared to the bulk [88]. This is particularly detrimental in

stainless steels because their resistance to corrosion is provided by the evenly distributed presence of chromium alloyed into the metal. However, as chromium combines with impurities such as carbon forming chromium carbides, the carbides precipitate out at the grain boundaries depleting the region of chromium and its protective properties [8-10]. This process, known as sensitization, can occur when the metal is heated to a temperature range of about 425 – 875°C [89]. When sensitized, the chromium depleted regions become very susceptible to corrosion especially when they are used in highly aggressive environments [89].

Several studies have shown that the special boundaries created during grain boundary engineering provide resistance to the problem of impurity atom segregation. Trillo and Murr [8] found that special boundaries in 304 stainless steel, specifically coherent twins (a type of  $\Sigma 3$  boundary), deter sensitization and precipitation of carbides at the grain boundaries because of their low interfacial energy. Precipitation was seen to occur and increase as grain boundary energy increased, thus, microstructures with dominant amounts of  $\Sigma 3$  twin boundaries would prevent sensitization in the material. Bi, et al. [9] also found that chromium depletion in grain boundary engineered 304 stainless steel at a lower-energy boundary ( $\Sigma 17$ ) was less than that of higher-energy general boundaries. Thus, frequent introduction of low-energy segments caused by twin-emission disrupted the continuity of chromium depletion along the boundary as well as the path of intergranular corrosion through material. Zhou, et al. [10] found that more than 90% of special boundaries ( $\Sigma \leq 29$ ) exhibited immunity to carbide precipitation in 304L stainless steel while only 20% of the general boundaries exhibited resistance. Aust, et al. [11] grain boundary engineered alloy 600 to several different special grain boundary fractions and found that even when sensitized (1 hr at 600°C), the corrosion rate for the highly grain boundary engineered sample was half that of the lesser sample because of the reduced sensitization effects at the more resistant grain boundaries.

Once sensitized, intergranular corrosion occurs at the grain boundary while the bulk of the grain remains unaffected because the segregation of impurities creates a difference in chemical makeup of the two regions [89]. However, grain boundary engineered materials

have been found to prevent this because of their large special boundary fraction. Lehockey, et al. [12] found that  $\Sigma 1$  grain boundaries in high purity aluminum were most resistant to intergranular corrosion with only 12 – 15% showing signs of attack while  $\Sigma 3$  boundaries fared slightly worse but not as bad as general boundaries, with 23 – 35% and 47 – 53% respectively showing susceptibility. Palumbo and Aust [13] studied Ni-3S finding immunity to intergranular corrosion at  $\Sigma 3$ ,  $\Sigma 7$ , and  $\Sigma 9$  grain boundaries when they had a deviation of the exact CSL angle of  $<1^\circ$ . Macroscopic studies of grain boundary engineered 304 stainless steel found the rate of corrosion reduced to a quarter of that in the original material [14]. Further studies found that increasing the frequency of special boundaries in Pb-alloy battery electrode grids decreased the weight loss due to corrosion by 26 – 46% [12] as well as the same dramatic effects in grain boundary engineered Alloy 600 [15].

### *1.3.2 Intergranular Cracking*

Stress-corrosion cracking of components is one of the most frequent and unpredictable causes of failure. However, grain boundary engineering has resulted in a more predictable microstructure with an even distribution of resistant (low- $\Sigma$  CSL) boundaries throughout. The key to the resistance of low- $\Sigma$  CSL boundaries is the low interfacial energy resulting from the high coincidence between crystal lattices concurrently making embrittlement less likely [11]. Studies have revealed that low angle boundaries ( $\leq 15^\circ$ ) in Ni-16Cr-9Fe did not crack and low- $\Sigma$  CSL boundaries were more crack resistant than general boundaries [16]. Pan, et al. [17] found that  $\Sigma 3$  boundaries were resistant to cracking but that other low- $\Sigma$  CSL boundaries were present in the crack path. However, these boundaries may not have been special when considering the boundary planes they resided on or if a different criterion for comparison to ideal CSL misorientations had been used. Gertsman and Bruemmer's [18] studies found similar results showing only twin ( $\Sigma 3$ ) boundaries were explicitly crack resistant when their interactions with general boundaries created barriers to crack advance. Grain boundary engineering also improved microalloyed steel's resistance to cold-work cracking and embrittlement through the addition of low- $\Sigma$  CSL boundaries because of the minimized solute effects and reduced interaction between interfaces and glissile dislocations [19].

### 1.3.3 Creep

Creep of FCC materials can also be significantly reduced by grain boundary engineering. During high temperature deformation, lattice dislocations interact with grain boundaries creating extrinsic grain boundary dislocations [20]. Grain boundaries can act as barriers to dislocation motion because they are natural discontinuities in orientation between grains, blocking dislocations as they reach the edge of the grain. However, general boundaries tend to easily absorb the dislocations (contributing to creep) while low- $\Sigma$  CSL boundaries do not (preventing creep) [21]. Thus, the introduction of a large percentage of low- $\Sigma$  CSL boundaries through grain boundary engineering can provide an effective solution to problems of creep. Lehockey and Palumbo [22] saw a factor of 16 reduction in creep rate when the special fraction of grain boundaries was increased from 13% to 66% in grain boundary engineered nickel. Was and Thaveeprungsriporn [21] obtained similarly dramatic results by grain boundary engineering samples of alloy 600 (Ni-16Cr-9Fe).

### 1.4 Grain Boundary Connectivity

Watanabe [23] noted that intergranular cracks may only propagate on general boundaries favorably oriented (near perpendicular) to the axis of the applied stress, and may be arrested at triple junctions comprised of two special boundaries. Figures 4 and 5 show this occurring. The red line in Figure 4 shows a propagating degradation such as intergranular corrosion or cracking along a path of general boundaries. When the crack encounters the two green, special boundaries at the triple junction, the degradation is halted from further propagation. Figure 5 shows this phenomenon as captured in an

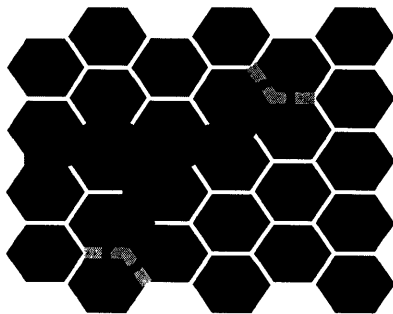


**Figure 4. Degradation along general boundaries halted at special boundaries.**

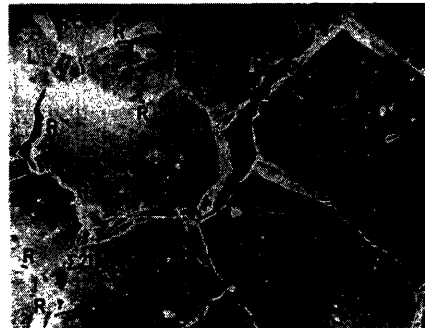


**Figure 5. SEM image of a crack halted by special boundaries [23].**

SEM. Therefore, the key to grain boundary engineering is to break the connectedness of this non-special, general boundary network so that cracks, corrosion, etc. cannot travel through the network degrading the material.

The simplest approach to accomplish this is to manufacture the materials in such a way as to promote the increase of special boundaries, concurrently decreasing the non-special boundaries and their connectedness. An example of an iterative progression on a microstructure is shown in Figure 6. As the process progresses, the general boundary network is shown to become fragmented as the boundaries are replaced by lower energy special boundaries.

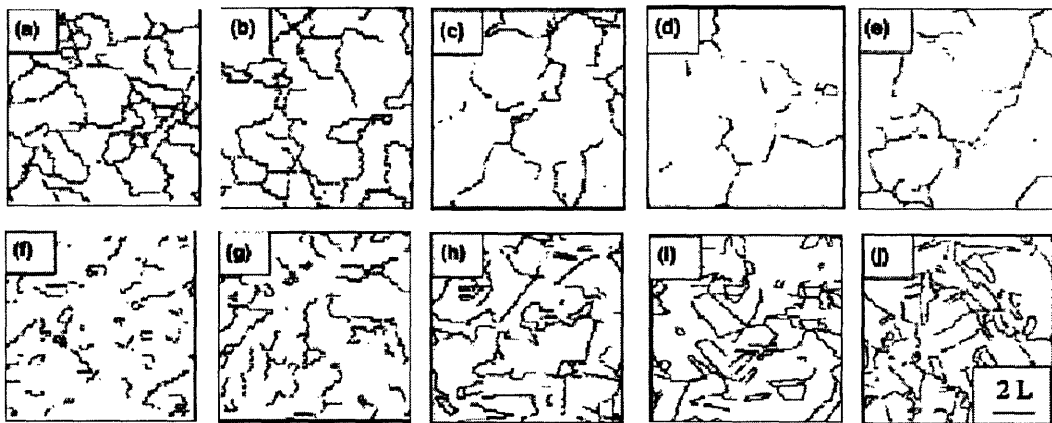


**Figure 6. Cycle by cycle images (a-e and f-j corresponding to 0, 1, 2, 3, and 4 cycles respectively) of the general grain boundary network (a-e) breaking up as the special boundary network (f-j) proliferates during a grain boundary engineering process [24].**

### 1.5 Grain Boundary Engineering Effectiveness

Grain boundary engineering a material to break-up the general boundary network requires a method to measure its effectiveness. Such a measurement parameter is essential because it will provide the differentiating factor between grain boundary engineering technologies and their respective intellectual property. The foremost parameter currently in use is the percentage of special boundaries either as a fraction of the total length or the total number of grain boundaries. For example, a stochastic model proposed by Palumbo, et al. [25] predicted the depth of intergranular cracking by

correlating the total fraction of special boundaries to depth of cracks seen in experiments. However, the model failed to accurately predict cracking in conditions where considerable twinning had occurred in the microstructure. Twins, generally the largest proportion special boundaries, can form in superfluous locations such as the center of grains where they contribute more significantly to length and number percentage statistics than to the breakup of the general boundary network. Some common twin formations are illustrated in Figure 7 where it can be seen that they have limited contributions because of their confinement to the grain interior. Lehockey, et al. [26] refers to these as “neutral” twins and provides a new model that discounts the contributions of “neutral” twins that are confined to grain interiors where they can be circumvented by other general boundary paths. However, models using the special boundary fraction will continue to have similar problems resulting from the preference of twin formations.

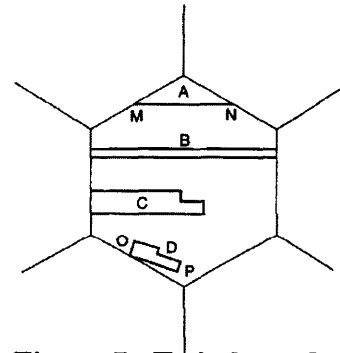


**Figure 7. Twin boundary formations that contribute much more significantly to length percentage statistics than to general boundary network breakup [27].**

Due to the factors described above, special boundary fraction is not a particularly good predictor of network topology and assessing the effectiveness of grain boundary engineering requires a more accurate parameter. Another such parameter that measures the distribution of triple junctions has been used to describe microstructural improvements arising from grain boundary engineering. As more triple junctions comprised of two special boundaries (type 2 junctions) are created in the microstructure, more general boundary paths for degradations to follow will become blocked, as illustrated in Figure 5. However, triple junctions statistics cannot characterize connectivity or path lengths so that even if the special boundary fraction and type 2 junctions are increased, an isolated chain of general boundaries could remain undetected.

While the special fraction of grain boundaries and the number of type 2 triple junctions increase when a material is grain boundary engineered, their values do not provide

assurance that the global connectivity of the general boundary network has been disrupted. Therefore, percolation theory has been applied to studies of grain boundary topology as a way to assess if there is connected path for degradations in the microstructure [78-80]. Percolation theory relies on the classification of network connections as either strong (special boundaries) or weak (general boundaries) and these classifications are assigned randomly through the microstructure that is being created [81]. Thus, in a simulated microstructure, it can be determined if a percolating path exists through the microstructure for the assigned special boundary fraction. In an infinite microstructure, the special fraction at which the network experiences a change from a percolating path to a non-percolating path is called the percolation threshold [82-84].

However, it has only recently been appreciated that crystallographic constraints require boundary misorientations to obey conservation rules around closed circuits and triple junctions, invalidating many uses of standard percolation theory [28]. These constraints make it so the topology of a general network varies greatly from more realistic networks as illustrated in Figure 8 below. Networks (a) and (d) were constructed using standard

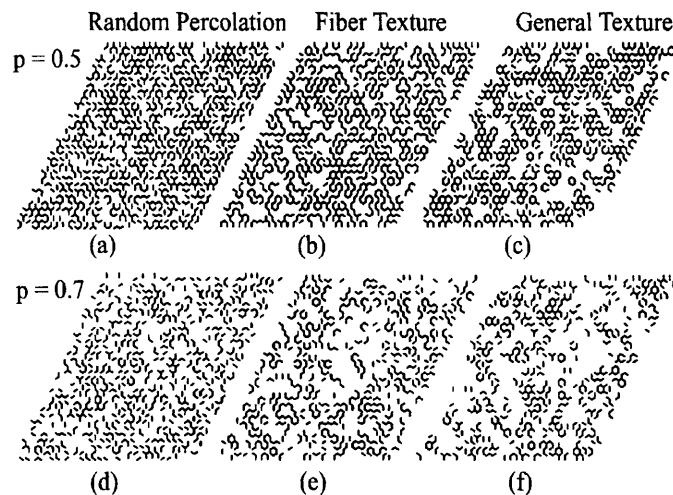


**Figure 8. Spatial distribution of a simulated high-angle (non-special) boundary network showing decreasing connectedness of non-special boundaries as percentage of special boundaries increases [28].**

percolation theory, assigning the general network with no regard for constraints and the fiber and general textures with the constraints in mind. In the randomly assembled

lattice, the spatial distribution of general boundaries is expectedly uniform, with no obvious tendency to cluster, whereas the crystallographically constrained tend to cluster together resulting in a patchier grain boundary network [28]. This tendency to form clusters of interconnected boundaries makes a measure of the total normalized length or “mass” of the clusters quite useful. This information can be pulled from EBSD data and analyzed to understand how grain boundary engineering decreases the mass and size of the general boundary clusters or increases that of the special boundary clusters. Schuh, et al. [24] developed algorithms to get a measure of the mean and maximum cluster mass, connectivity length and maximum linear dimension. It appears that measures of cluster parameters could be the most accurate way to quantify the effectiveness of a grain boundary engineering process. This could prove to be invaluable to the commercialization of the technology by challenging current intellectual property and providing insight into more effective and possibly new grain boundary engineering processing techniques.

## 2. Processing and Manufacture

### 2.1 Introduction

Grain boundary engineering is accomplished through iterative thermomechanical processing, i.e. cyclic straining and annealing of face-centered cubic (FCC) materials. The most common of these include stainless steel, nickel, copper, lead and their various alloys. Grain boundary engineering is limited to FCC materials with low stacking fault energy, which allows  $\Sigma 3$  twins to proliferate easily [87]. For this reason, twins account for the largest part of the special boundary fraction increase in nearly every case, leading to the more accurate label of twinning-related grain boundary engineering [31]. As evidenced in the previous section, twin boundaries are resistant to segregation, corrosion and cracking, making their plentiful nature extremely useful. The two types of grain boundary engineering, strain annealing and strain recrystallization, use distinctly different processing routes. However, their underlying improvements are provided through similar mechanisms and grain boundary engineering through either process can be accomplished as long as twin generation can take place [31].

#### *2.1.1 Strain Annealing*

Strain annealing is characterized by low levels of strain, typically on the order of 5 – 10%, followed by at least an hour, but more commonly, a several hour long anneal [31]. Further, the annealing temperature must be low enough to prevent recrystallization of the grains but high enough to allow grain boundaries to rearrange into lower energy configurations (low- $\Sigma$  CSL boundaries) [34]. However, two aspects of this processing make it less desirable for commercialization: the multi-hour annealing time would slow production and consume significantly more furnace power per pound of material produced; and the annealing treatments lead to considerable grain growth which tends to lower the material's strength.

Many studies have examined the effects of strain annealing on various pure metals and alloys. Table 1 summarizes the best of the results from several studies examining strain annealing processing. The results have only limited usefulness because their

standardized method for quantifying effectiveness is the resultant special boundary fraction. As explained in the first section, this parameter is not able to completely determine the effectiveness of the process in breaking the connectedness of the material's general boundary network. Thus, even though some results show very low or very high special boundary fractions, a true determination of the success of a grain boundary engineering processing schedule cannot be determined from these statistics. The table does show the wide variety of processing schedules that have been attempted as well as the many materials that have been studied.

Paper #	Material	# of cycles	Reduction Percentage	Annealing Temperature (Celsius)	Annealing Time	Initial Grain Size	Final Grain size (micron)	Initial % CSL	Final % CSL	Total % CSL change	% Sigma 3	Reference
1	304 Stainless Steel	3	3%	950	10 min	24	-30	34	57	23	50	[32]
2	99.99% OFE Copper	2	6%	275 and 375	14 h, 7 h	-	65	70	85	15	67	[33]
3	Ni-200 (99.5% Ni)	1	6%	900	10 min	-	60	36	75	39	60	[34]
4	Alpha Brass	2	15%	620	15 min, 1hr	-	NA	42	68	18	8	[35]
5	Alloy 600 (Ni-16Cr-9Fe)	3	5, 3, 2%	890, 890, 936	6, 20, 11 h	-	330	-	28 - 43	-	-	[21]
6	304 Stainless Steel	1	5%	1200	72 hr	16	31	-	86.5	-	-	[14]
7	Alloy 600/690 (Ni-16Cr-9Fe-xC)	3	3%	925	7.5 min	35	-	-	70	-	-	[36]
8	99.999% Ni	2	6%	850	168, 24 hr	-	-	-	-	-	32	[37]

**Table 1. Summary of strain annealing processes.**

Deformation plays an important role in the strain annealing process. Under strain, grains subdivide forming general, high angle boundaries leading to decreases in the special boundary fraction [34]. However, these deformation-induced structures provide the necessary driving force to form new special boundaries during the heat treatment [33, 37], but it is necessary to find the correct balance and the proper amount of strain. Too much strain can lead to complete recrystallization of the grains (depending on the temperature) destroying the old microstructure, which is more conducive to special boundary formation. Thus, an optimized amount of strain must be applied that is based on the type of material as well as the length and temperature of the annealing step. Studying one-step treatments, Lee and Richards [34] found that commercially pure nickel strained 6% and annealed for 10 minutes at 900°C produced the most special boundaries when optimizing between 3 – 12% strain and 500 – 900°C. Another one-step processing investigation similarly found that a modest 5% strain was optimal because

recrystallization was suppressed, preventing the creation of general boundaries that cannot reconfigure during the single annealing step [14].

### 2.1.2 Strain Recrystallization

The second type of grain boundary engineering processing, strain recrystallization, is characterized by a medium level of deformation, typically around 20-30%, followed by an anneal above the recrystallization temperature (typically 0.6-0.8 of the melting temperature) but only for a few minutes [31]. This approach sidesteps the excessive annealing time and grain growth drawbacks of strain annealing making it the most promising for commercialization. Table 2 summarizes several investigations into strain recrystallization processing. Palumbo, et al. [41] have already patented a wide range of strain recrystallization processing schedules and the ramifications of this for commercialization of other grain boundary engineering techniques will be discussed in the next section.

Paper #	Material	# of cycles	Reduction Percentage %	Annealing Temperature (Celsius)	Annealing Time (min)	Initial Grain Size (microns)	Final Grain Size (microns)	Initial % CSL	Final % CSL	Total % CSL change	% Sigma	Reference
1	Copper	3	30%	375	10	-	27	-	75	-	60	[38]
2	Copper	3	20 - 30%	350 - 400	10	~125	-	20	63	43	31	[39]
3	Copper	4	20%	560	10	-	-	37	68	31	52	[40]
4	Inconel 600	7	20%	1000	15	-	-	37	65	28	33	[39]
5	Inconel 600	4	25%	1025	18	-	-	43	62	19	-	[24]
6	Inconel 600	3 - 7	5 - 30%	900 - 1050	2 - 10	-	<30	-	>60	-	-	[15] and [41]
7	Inconel 718	4	20%	1050	60	-	74	21	41	20	34	[42]
8	Nickel	1 - 3	2 - 10%	750-900	10	-	50 - 200	50 - 65	-	45 - 55	-	[43]
9	Alpha Brass	5	25%	665	5	-	54	-	42	34	-	[44]
10	Lead	2 - 3	30%	270	10	-	25 - 60	33	92	59	68	[45]

**Table 2. Summary of strain recrystallization processes.**

As mentioned earlier, one of the main differences between the strain annealing and strain recrystallization methods is the number of cycles necessary. Strain annealing generally requires a maximum of three iterations although it is often accomplished with less. References [46] and [14] demonstrate a moderate rise in the special boundary fraction without using a deformation step. However, references [14] and [34] found that single-step processing is optimized with the inclusion of the deformation step. Strain recrystallization processing generally requires at least three and in some cases seven

iterations to change the grain boundary character distribution (GBCD) sufficiently. In this way, cycling is the crucial condition for producing increases in the special boundary fraction of metals during strain recrystallization processing. The effect of iteration is shown in Figure 9, which illustrates the increase in CSL fraction with each processing cycle for several investigations of twin-related grain boundary engineering [31]. Although the trends of low- $\Sigma$  CSL boundary fraction between iterations one and two can be seen to be quite erratic, subsequent iterations show increases in all cases demonstrating multiple iterations are undeniably important.

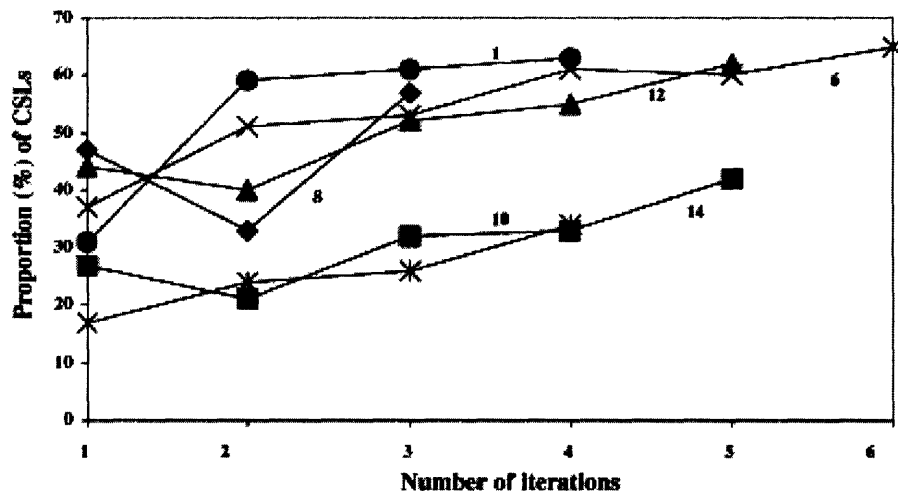


**Figure 9: Proportion of low- $\Sigma$  CSL boundaries vs. number of processing iterations for several relevant twin-related grain boundary engineering investigations showing an inconsistent trend between the first and second cycle but consistent increases thereafter [31].**

Randle [47] suggests the behavior of  $\Sigma 3$  twins is responsible for the erratic special boundary fraction resulting from the first two processing cycles. She offers that initially twins retain strain as dislocations pile-up, increasing the internal stress and recrystallization driving force. The rise or drop in special fraction during the first two cycles likely depends only on the initial microstructure of the material. Some twins and dislocations are wiped out as mobile boundaries sweep through allowing annealing twinning to occur. Twins form and proliferate, generating more and more  $\Sigma 3$  twins that break up the general boundary connectivity and achieve a grain boundary engineered material.

## 2.2 Intellectual Property (IP) Review

As previously discussed, current grain boundary engineering processing techniques are composed of thermomechanical cycles, i.e. a deformation or straining process such as rolling followed by an anneal. Since these processes are already necessary conditions for the manufacture of most products in the steel or metal alloy industry and anyone with these capabilities and grain boundary engineering processing knowledge could begin producing a grain boundary engineered product. Thus, intellectual property is vital to protect emerging grain boundary engineering technologies.

### *2.2.1 Grain Boundary Engineering IP*

Grain boundary engineering IP generally stipulates several processing variables as well as an effectiveness parameter measured at the process's completion. The differentiating variables include the material, forming reduction percentage, annealing time, annealing temperature, and the number of cycles. The effectiveness parameter is generally a measure of a particular grain boundary type (i.e. special, low angle,  $\Sigma 3$ , etc.) achieved at process completion and a minimum fraction of this boundary is specified to be obtained if the processing schedule is followed. In many cases, the resulting grain size of the material is also stipulated because of its effect on the material's strength.

There are only a handful of registered patents for grain boundary engineered processes. However, Integran Technologies Inc. (or one of its founding members) owns over half of these patents as well as the trademark GBE® (grain boundary engineered). Several of the patents including #6,802,917, #6,592,686, and #6,342,110 are for a method of grain boundary engineering a lead alloy for electrodes in lead-acid batteries. Two others relate to a grain boundary engineered surface treatment (#6,344,097) and a process for grain boundary engineering Ni- and Fe- based superalloys (#6,129,795). Although these last two do not immediately encroach upon the commercial aim of this evaluation, they will be discussed because of their possible relevance to niche applications that could develop for grain boundary engineered product. Another Integran patent (#5,817,193) [41] as well as a Japanese patent (JP2003253401) and a US patent application (US 2004/0156738 A1) appear to be the only patent protected grain boundary engineering

processes truly relevant to this evaluation. These, along with the two other Integran patents, will be examined to understand their claims, processing methods, and consequences in relation to obtaining new grain boundary engineering IP.

#### *2.2.1.1 United States Patent #5,817,193*

Integran's most commercially viable patent is United States Patent #5,817,193 entitled *Metal Alloys Having Improved Resistance to Intergranular Corrosion and Stress Corrosion Cracking* [41]. Dated Oct. 7, 1998, it provides processing parameters for the "fabrication of components from a face centered cubic alloy, wherein the alloy is cold worked and annealed, the cold working is carried out in a number of separate steps, each step being followed by an annealing step. The resultant product has a grain size not exceeding 30 microns, a "special" grain boundary fraction not less than 60%, and major crystallographic texture intensities all being less than twice that of general values. The product has a greatly enhanced resistance to intergranular degradation and stress corrosion cracking, and possesses highly isotropic bulk properties." The main claim of this patent is that by subjecting an austenitic stainless, iron-based or nickel-based face centered cubic alloy to at least three cold working and annealing cycles wherein the forming reduction is between 5% and 30% is followed by an annealing step at a temperature in the range of 900-1050°C for a time of 2-10 minutes, an alloy will be produced with a randomized grain texture, enhanced resistance to intergranular degradation, and increased special grain boundary fraction of at least 60%.

This patent is very broad from the standpoint that it covers almost all relevant FCC materials for a wide range of strain recrystallization processing conditions. Although it does not claim any method of breaking up the connectivity of the general boundary network, its claimed improvement to a 60% special boundary fraction may automatically put it in a regime insuring connectivity break-up even without any elicited measurement. This patent could result in claims of infringement if its processing conditions are encroached upon by newly developed IP.

#### 2.2.1.2 Japan Patent JP2003253401

Japan patent JP2003253401 dated Sept. 10, 2003 entitled *Austenitic Stainless Steel Excellent in Intergranular Corrosion Resistance and Production Method Thereof* [63] is registered to several prominent Japanese grain boundary engineering researchers and JFE Steel KK as the patent applicant. It claims a process for producing an austenitic stainless steel exhibiting improved intergranular corrosion resistance possessing a total fraction of special boundary length of greater than 70% of the total grain boundary length. The process specifies parameters consisting of a single cold rolling step of 2 – 15% followed by an anneal at 900 – 1000°C for greater than five hours.

This patent does not cover nearly as many of the processing variables for strain annealing as the previous patent did for strain recrystallization processing. It only specifies austenitic stainless steels instead of austenitic stainless, iron-based or nickel-based face centered cubic alloy. Likewise, it only specifies a single step process at greater than 5 hours. This, if a multiple step but shorter annealing cycle process could be proven effective, IP could be obtained without encroachment upon this patent. However, as mentioned before, strain annealing is not likely as promising because of slower production rates and significant grain growth, which likely explains the dearth of IP.

#### 2.2.1.3 United States Patent Application Pub. No. US 2004/0156738 A1

United States Patent Application Pub. No. US 2004/0156738 A1 entitled *Nickel Alloy and Manufacturing Method for the Same* [64] was published Aug. 12, 2004. Manabu Kanzaki and Amagasaki-shi are listed as inventors but have not appeared in any grain boundary engineering research or literature and thus no information is known about them. The patent claims a nickel alloy processed such that the low angle boundary rate is increased to greater than 4% exhibits an excellent resistance to intergranular stress corrosion cracking. A low angle boundary is specified as a grain boundary, which has a grain boundary orientation difference between 5 degrees or more and 15 degrees or less. Processing conditions are specified for two different nickel alloys: a single cold working reduction of 60% or more for a nickel alloy of mass % C: 0.01-0.04%; Si: 0.05-1%; Mn: 0.05-1%; P: 0.015% or less; S: 0.015% or less; Cr: 25-35%; Ni: 40-70%; Al: 0.5% or

less; Ti: 0.01-0.5%; or a single cold working step of 40% or more followed by an heat treatment determined by the equation  $(\text{Reduction } \%) * (0.1 + 1/\exp[\text{Temp}/500]) \geq 10$  for a nickel alloy of mass % C: 0.01-0.05%; Si: 0.05-1%; Mn: 0.05-1%; P: 0.02% or less; S: 0.02% or less; Cr: 10-35%; Ni: 40-80%; Al: 2% or less; Ti: 0.5% or less. The second process does not stipulate the time length of the heat treatment.

This patent tries a different route from strain annealing or strain recrystallization in that it uses very high forming reductions to manipulate the GBCD and improve corrosion resistance. Low angle boundaries can be a byproduct of traditional grain boundary engineering methods although they are typically not measured at the completion of processing. This method of processing may increase the special boundary fraction to the levels of the previous patents just using very high forming reductions instead of cyclic straining and annealing. In either case, this patent could possibly restrict another chunk of processing conditions if granted approval.

#### *2.2.1.4 United States Patent #6,129,795*

Another of Integran's patents is United States Patent #6,129,795 entitled *Metallurgical Method for Processing Nickel- and Iron-based Superalloys* [65]. Dated Oct. 10, 2000, this patent claims "a method for processing a precipitation-hardened austenitic Ni- and Fe-based superalloy to increase the fraction of special low- $\Sigma$  grain boundaries to a level greater than 50%." The first two deformation steps must be 10% and 20% cold deformations with each followed by an annealing step in the range of 1100 – 1300°C for one to eight hours. The final cycle is also specified and must comprise a cold deformation of 5 – 10% with a subsequent anneal between 700 – 900°C for up to 16 hours.

This patent shouldn't encroach upon the aim of grain boundary engineering as described in this evaluation. Since it focuses on precipitation based superalloys, it requires very long annealing steps so that processing times may take in the range of days. However, a product made in this manner could be sold for a significant premium due to its enhanced resistance to high temperature degradation including creep and hot corrosion. Further, it

mentions a property of enhanced weldability that could allow for better integration into a variety of products and shapes due to its ease of joining.

#### *2.2.1.5 United States Patent #6,344,097*

Integran's patent #6,344,097 dated Feb. 5, 2002 is entitled *Surface Treatment of Austenitic Ni-Fe-Cr-Based Alloys for Improved Resistance to Intergranular-Corrosion and Cracking* [66] protects a process for grain boundary engineering a material as a final surface treatment step. Cold working would be applied as some form of peening (shot, laser, hammer, etc.) to cold work the near surface region to a depth in the range of 0.01 mm to about 0.5 mm so that the bulk material is unaffected. The annealing step requires a temperature greater than 900°C but below the melting point for a time sufficient to induce recrystallization of the near surface region. Specific applications mentioned include nuclear steam generator tubing or nuclear reactor core head penetrations. The patent does not have any mention of special boundaries or a critical special boundary fraction; however, grain boundary engineering is responsible for the expected improvement in material property.

Again, this patent shouldn't encroach upon the aim of grain boundary engineering as described in this evaluation as it focuses on a surface treatment instead of the bulk material. However, it is a novel process that aims to improve possible niche product areas that could compete in the same markets and application areas.

#### *2.2.2 Intellectual Property Strategy*

In order to commercialize grain boundary engineering technology, grain boundary engineering intellectual property must be obtained. As mentioned in the first section, the grain boundary special fraction measurements as claimed in the relevant patents above are not entirely accurate predictors of grain boundary engineering effectiveness. For this reason, Professor Schuh and his research group are working to understand the underlying grain boundary network constraints and could develop a much more accurate parameter to judge grain boundary engineering effectiveness. This optimized processing parameter would have to be one of the central claims in establishing new grain boundary

engineering IP. However, winning patent approval and avoiding possible litigation could be obstacles during this process.

The United States patent system differentiates patents by their stated claims. Grain boundary engineering patents generally use product-by-process claims wherein they state the grain boundary engineered metal will contain at least a minimum fraction of special boundaries when it is produced using the specified variables. Since the most obvious and overarching process variables have already been guarded with IP, a new patent could only be established if sufficiently different processing results could be claimed from a grain boundary engineering process. Essentially, this will come down to developing a new parameter, likely based on grain boundary network connectivity, to show grain boundary engineering effectiveness in ways the boundary fraction parameter fell short. Hopefully, this new effectiveness parameter can then show that other IP claims inadequately assumed a grain boundary engineered material resulted from the specified process variables. For example, United States Patent #5,817,193 [41] claims its process results in a special boundary fraction of at least 60%. If a new parameter can show remarkably different microstructures (i.e. substantially different general boundary connectivity even above the stated boundary fraction criterion) resulting from slightly overlapping processing variables and minimum boundary fraction claims do not adequately capture these aberrations, new IP may be able to be established.

New patent applications must be filed within one year of publishing in a public forum in order to qualify for application status. While this should not be a problem, infringement upon prior patents is very likely if the process variables significantly overlap those of existing grain boundary engineering IP. Existing IP meets the requirements to be a single piece of prior art and thus qualifies for what courts have established in prior patent law rulings as the Doctrine of Equivalence. This permits infringement to be found even where the accused process does not literally infringe on previous patent claims and can be ruled if each element of the claimed invention has a substantial equivalent in the accused process or if the difference between each element in the accused process and the claim elements are insubstantial [61]. In court cases similar to this type of infringement, the

Federal Circuit has stated that “to be a substantial equivalent, the element substituted in the accused product for the element set forth in the claim must not be such as would substantially change the way in which the function of the claimed invention is performed” [61]. Thus, claims of a new effectiveness parameter differentiating between grain boundary engineering processes could be left to the decision of litigation and ultimate court ruling because although more accurate, a new parameter may assess results comparable to that of grain boundary special fraction.

Licensing could be a viable option for realizing the commercial potential of grain boundary engineering technologies in two different ways. Either a new company could license grain boundary engineering IP that has already been established if they are confident that their market knowledge and position would allow them to profit even when they are paying licensing fees. This may be a difficult proposition requiring special knowledge of a specific application that has gone untapped by the rest of the industry as well as a large capital investment to begin production operations. On the other hand, if new grain boundary engineering IP is successfully established, it could be licensed out to make the technology profitable without the significant risk of capital investment that accompanies the self-commercialization of the technology. This offers a much more modest risk-reward position but nonetheless a positive possibility.

### 2.3 Processing Analysis

Grain boundary engineering can be performed using many different forming processes including rolling, forging, or extrusion, as long as it consists of shaping steps to strain and form the product and annealing steps to reduce the residual stresses. This could make grain boundary engineering applicable to several products and shapes including sheets, bars, rods, or tubes. Figure 10 illustrates several common shape forming processes that could accomplish grain boundary engineering.

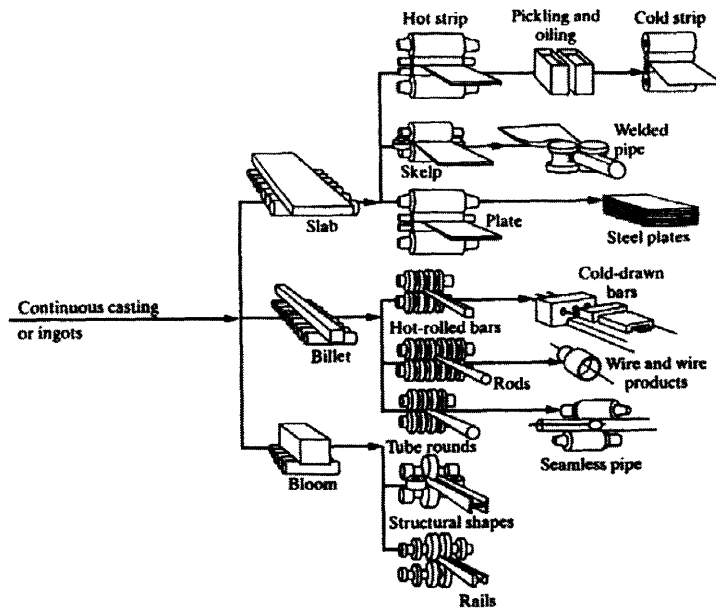


**Figure 10. Schematic outline of various flat- and shape-rolling processes [30].**

The analysis for this evaluation focuses on a continuous sheet metal production process consisting of rolling, annealing, and cooling. However, it might also provide insight into the potential scale-up of other grain boundary engineered products or shapes because of the general processing similarities. The goal of this analysis is to show the relationships between the many processing variables and the manufacturing line requirements and dimensions to get a sense of the general order of magnitude for the relevant design criteria. Although each of these manufacturing processes are well understood and can be calculated with sufficient accuracy using the calculations detailed in Appendix A, many of the inherent characteristics of the line had to be approximated and thus all of the following numbers are at best estimates to provide a general approximation.

### *2.3.1 Benchmark Processing Conditions*

When considering a manufacturing line for grain boundary engineered materials, the length of the line, production rate, and processing time are important factors. Each of these is affected by variables in the grain boundary engineering process including the material, production line speed, number of cycles, amount of strain, annealing temperature, and annealing time. To provide a basis for comparison for each variable as it is examined, a 4 cycle process with 15% strain, annealed for 10 minutes at 950°C was

set as a benchmark because it represented the median conditions of the primary strain recrystallization patent [41] discussed earlier. The analysis also assumes production of type 304 stainless steel formed into 20-gauge sheet (~0.91 mm) with rolling mills having 200 mm diameter work rolls. Since the production rate of the line is only dependent upon the final speed at which the sheet emerges from the process, the sheet velocity was set to result in production rates of 10, 100, and 500 tons per day (using production line speeds of about 10, 100, and 500 fpm respectively). These production rates result in total productions of 2200, 22,000, and 1,100,000 tons per year respectively which would capture about 0.1%, 1%, and 6% of the market in the US for stainless steel sheet/strip (~1,800,000 tons in 2004) [62].

### *2.3.2 Individual Cycle Analysis*

Due to the conservation of volume, as the sheet is strained and deformed during each rolling cycle, the sheet's velocity changes accordingly. Since rolling is assumed to change only the thickness of the sheet, the conservation equation reduces to:

$$V_i h_i = V_o h_o.$$

where  $V_i$  and  $V_o$  are the initial and final velocities and  $h_i$  and  $h_o$  are the initial and final thicknesses. Thus for a deformation of 10%, the sheet speed upon exit will have increased by a factor of 1.11. This increase in sheet velocity results in cycle-to-cycle changes in annealing cycle time, furnace length, furnace power consumption, and rolling power required. The general trends and relationships of these will be illustrated and discussed in the following paragraphs.

The most important design factor for a grain boundary engineering processing line is its length because this directly affects the power required to heat the furnace as well as the furnace's capital cost. For the benchmark processing conditions, the length of the line increases as production rate increases. This increase is because the line speed increases significantly at higher production rates causing the sheet to travel longer distances during heating and annealing. The rolling and cooling cycles of the process also require longer

distances but are at least an order of magnitude smaller than the furnace and thus can be neglected in comparison to the length estimates of the annealing cycle. Figure 11 shows the changes in furnace length for each cycle. Later cycles require longer furnaces because of the increased speed of the sheet.

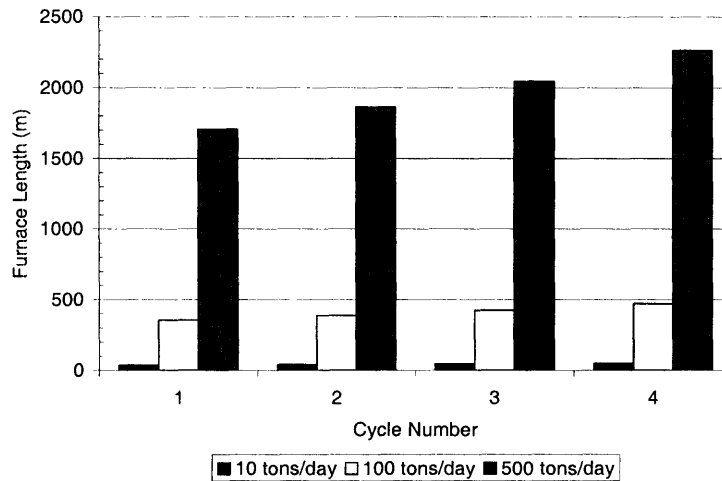


**Figure 11. Furnace lengths for each cycle.**

As mentioned previously, the length of the furnace is important because longer furnaces require more radiant tubes to transfer heat, thus burning more fuel and consuming more power. Since larger production rates require longer furnaces, they also require considerably more power. The increased power consumption in later cycles due to longer furnace requirements also is shown in Figure 12.

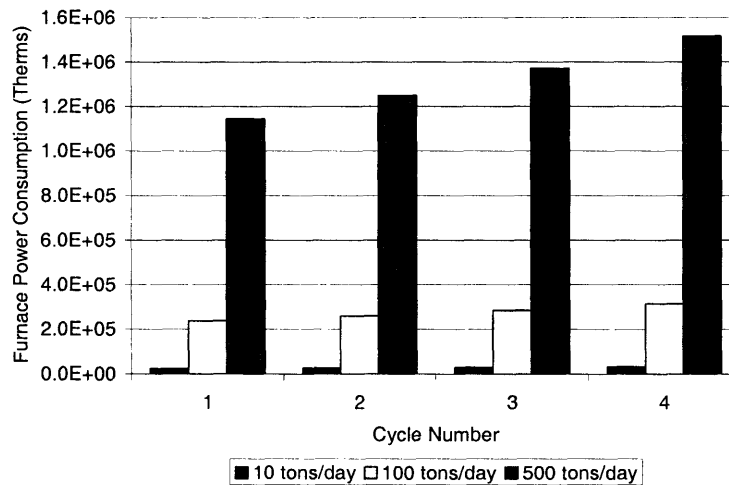


**Figure 12. Furnace power consumption for each cycle.**

The time required to traverse the production line varies only slightly for the three production rates. This time is determined almost solely from the time required for the annealing cycle. Although the anneal is set for 10 minutes every cycle, the time required for the sheet to warm up to the annealing temperature varies as the sheet's thickness changes, i.e. it heats more quickly as the sheet is thinned. Further, the annealing time decreases somewhat as the production rate increases because the increased velocity of the sheet expedites convective heat transfer to the sheet. Both of these trends are shown in Figure 13. The rolling and cooling steps add only seconds to each cycle and are assumed to be negligible when combined with the several minute annealing time estimates.

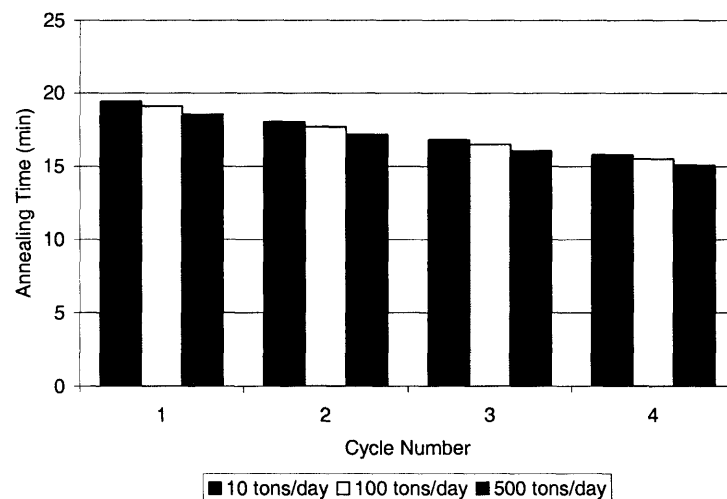


**Figure 13. Annealing times (including warm up) for each cycle.**

Rolling power consumption also increases as the production rate increases because the rollers must rotate at higher RPMs to deform the materials more quickly at the increased sheet velocity. The power also increases with each rolling cycle due to the cycle-to-cycle increase in sheet velocity although it is barely perceptible from Figure 14.

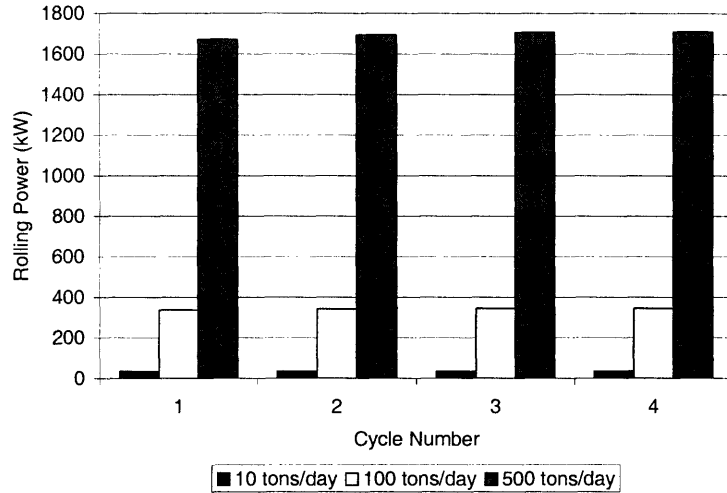


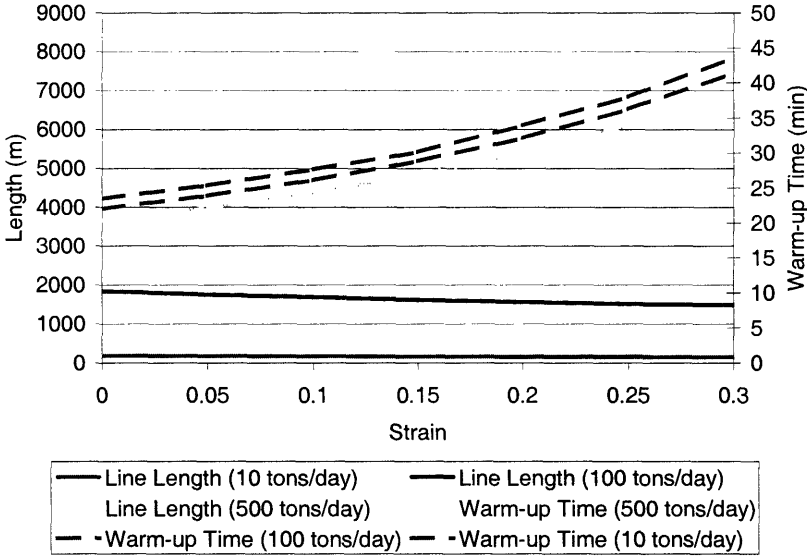
**Figure 14. Rolling power consumption for each cycle.**

### 2.3.3 Individual Variable Analysis

As previously mentioned, the most important design factor for a grain boundary engineering processing line is the length of the line because it directly affects the power consumption of the furnace as well as the furnace’s capital cost. The time required to heat to the annealing temperature is a key component of the furnace length, so it is useful to evaluate the effect of different processing variables on this as well. This section aims to estimate the order of magnitude of the furnace length and the time to warm-up to the annealing temperature while holding the other conditions at their benchmark values. It also illustrates the consequences of varying the processing conditions including the number of cycles, strain, annealing time and annealing temperature to find the resulting effect on furnace length and warming time.

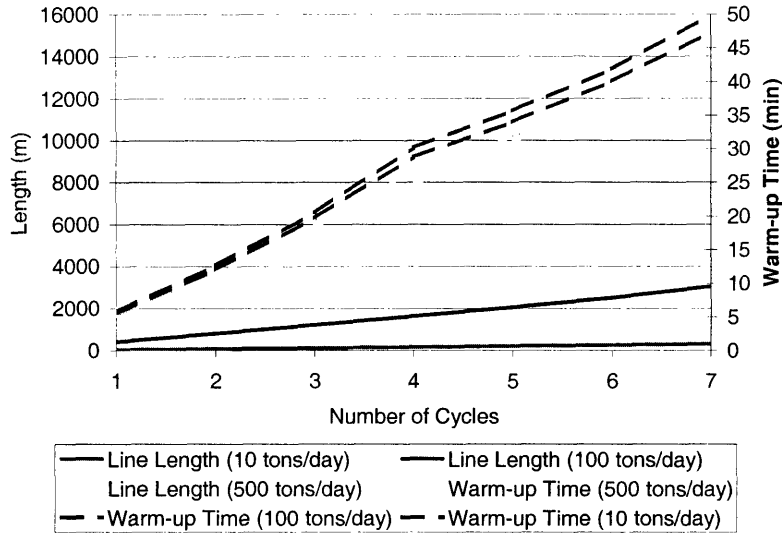
Figure 15 shows the effect the amount of strain in the grain boundary engineering process has on the furnace length and the warm-up time. The furnace length decreases with increasing strain because larger strains create greater variations in sheet velocity resulting in slower initial velocities when the production rate is fixed (meaning the final velocity is also fixed). With slower velocities in the first few cycles, the sheet does not need to travel as far during the annealing cycle and the length of the line decreases. The furnace power consumption follows this same trend because the number of radiant tubes burning fuel decreases as the length of the furnace decreases. The time required to warm-up to

the annealing temperature increases as strain increases. This is because larger strains require thicker initial sheets that require more energy to heat to the annealing temperature. Further, the time to warm the sheet decreases with increasing production rate because a higher velocity increases the heat transfer to the sheet by increasing convective heat transfer. Rolling power remains nearly constant at about 0.003 kW for all production rates and strains and thus is not illustrated.



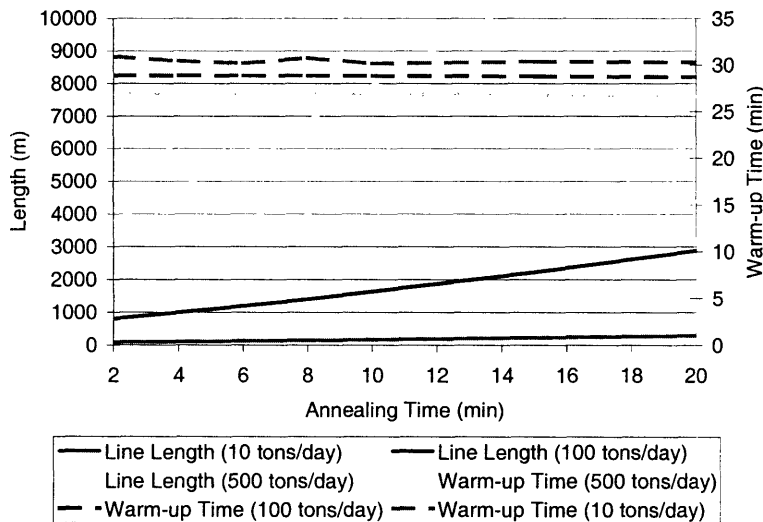
**Figure 15. Furnace length and time to warm to the annealing temperature as a function of strain and production rates.**

Figure 16 shows the variation in total length and warm-up time relative to the number of cycles required for the process. The trends are exactly as would be expected showing each to increase as additional cycles are added. The figure also provides rough estimates for necessary size of the each many cycled processing line and furnace required for the benchmark processing schedule.



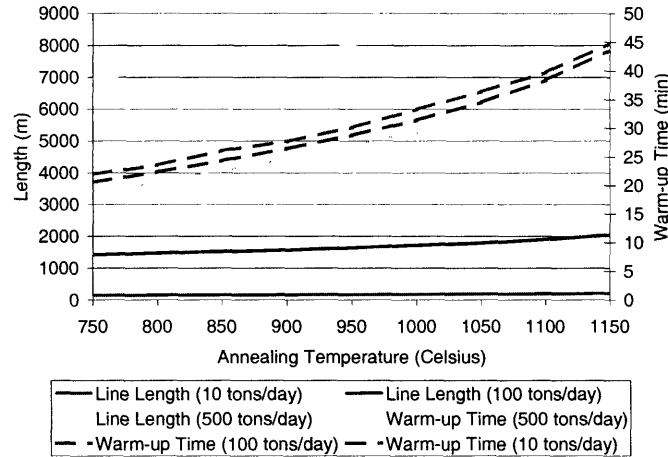
**Figure 16. Rough estimate for length and warm-up time required for the benchmark process with varied numbers of cycles.**

Figure 17 shows the variation in total length and warm-up time relative to the length of the annealing cycle. The furnace length obviously increases because it travels further during the increased annealing time. The time to warm to the annealing temperature changes with production rate because the increased sheet velocity increases convective heat transfer. Again, the figure provides rough estimates for the necessary size of the processing line and furnaces required for the benchmark process with varied annealing times.



**Figure 17. The length of the furnace increases but the time to warm to the annealing temperature remains nearly constant with varied annealing**

Figure 18 shows that the furnace length and time to warm to the annealing temperature each increase as the annealing temperature is increased. The furnace length will vary from the benchmark length by the shortage or excess of length traveled while warming to the desired annealing temperature.



**Figure 18. The length of the furnace and time to warm to the annealing temperature increase as the annealing temperature**

### 2.3.4 Strain Annealing Analysis

Strain annealing processing could be an option instead of strain recrystallization processing for grain boundary engineering. As described before, this could only be viable for lower production rates because it requires hours of annealing rather than minutes. For this analysis, Japan Patent JP2003253401 was used as the benchmark to evaluate feasibility because it is the chief strain annealing patent. The patent stipulates a single cold rolling step of 2 – 15% followed by an anneal at 900 – 1000°C for greater than five hours.

Figure 19 shows the length of the line for several production rates. If production rates are set low enough, strain annealing appears to be a viable commercial option because furnace lengths will not be absurdly long. Figure 19 also show that if a strain annealing process was developed that required less than 5 hours per annealing cycle, strain annealing processing could become more promising, at least when only considering line length.

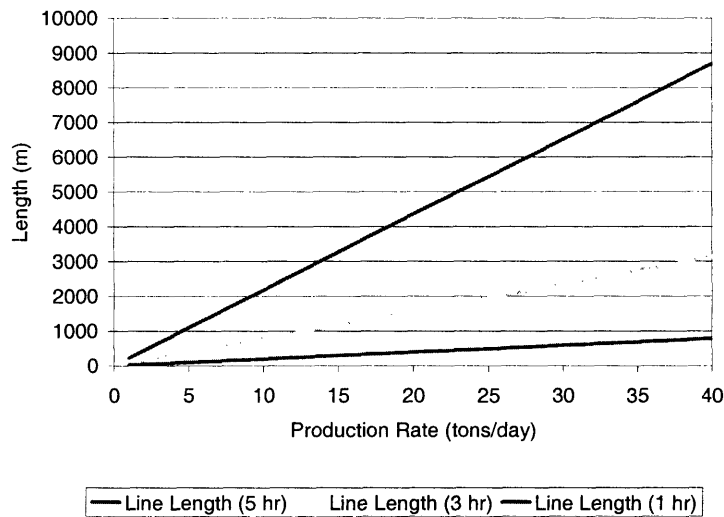


**Figure 19. The length of furnace required for strain annealing processes with annealing cycles of 1, 3, and 5 hours.**

### **3. Market Analysis, Competition, and Cost Analysis**

#### 3.1 Market Analysis

Grain boundary engineering has been shown to improve a wide variety of properties in FCC materials including electromigration [67], dynamic embrittlement [68], cleavage cracking [69], plasticity [70], electrical conductivity [71], and superconductivity [72] as well as solute segregation, intergranular corrosion, intergranular cracking, and creep as discussed in chapter 1. In most cases, the examinations have focused on improvements of properties in the high-end materials exposed to extreme environments. For example, grain boundary engineering has been shown to improve nickel- and iron-based superalloys in several ways. Alloy 738, alloy 625, and alloy V-57 are used in jet engines, gas turbine components, or rotors because of their extremely high resistance to temperature, corrosion, fatigue and creep damage. By grain boundary engineering samples of each of these materials, the maximum intergranular attack depth from hot corrosion tests was halved as compared to the non-grain boundary engineered base samples [76]. Further, the three alloys' cycles-to-failure significantly increased and the creep rate of alloy V-57 was reduced 15-fold [76].

However, just about any product comprised of an FCC material could be improved by grain boundary engineering and not all applications require the top end improvement mentioned in the previous paragraph. The technology could also provide significant performance improvements for the midrange of materials, possibly allowing them to become competitive and usable in applications that previously required more specialized materials. One of the most common these midrange FCC materials is stainless steel. Austenitic (FCC) types compose the 300 series of stainless steels and make up ~70% of the stainless steel market. Stainless steels are widely used because of their corrosion and temperature resistance, ease of fabrication and competitive cost as compared to other metal options. Typically, as you progress through the series to the higher grades of stainless steels, they become more resistant to degradations. For example, Figure 20 shows that type 304 experiences higher rates of corrosion than types 316 or 317.

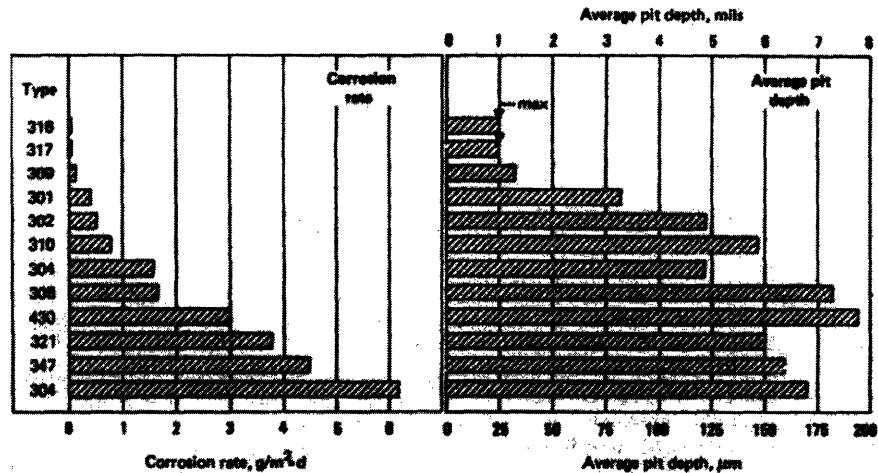


Figure 20. Corrosion of stainless steels in an industrial atmosphere [75].

The greater resistance of higher grade alloys is typically conferred by changing the base material's makeup through alloying or the removal of impurities and each type within a particular series of stainless steels will be characterized by a different elemental composition. Type 304 is the most widely used type within the series due to its good resistance to elevated temperature as well as adequate corrosion resistance. Type 305 has increased nickel content making it more stable at high temperatures. Types 316 and 317 add molybdenum resulting in greater resistance to corrosion and more stable mechanical properties at high temperatures. Types 309, 310 and 314 have much more chromium and nickel providing for their usage in high-temperature, corrosive environments. Type 347 contains niobium and tantalum while type 321 contains titanium making them useful in welded components where a high resistance to stress corrosion cracking is necessary. The L-series of stainless steels (such as 304L or 316L) rely on extensive purification and removal of carbon from the alloys to provide greater resistance. With the advent of grain boundary engineering, there is now a new way of improving corrosion susceptibility without the need to alloy or remove impurities. Therefore, grain boundary engineered materials could be very competitive against these other options because they do not require the addition of expensive alloying elements or costly impurity removal processes.

The world market for stainless steel is growing steadily at about 5% per year but China accounts for nearly 75% of this growth [73]. Predictions estimate it will top 25 million

tons in 2005 with over 70% of the total being austenitic (FCC). Assuming a conservative average price for stainless steels of about \$1.50 per lb, the world stainless steel market can be estimated to be at least a \$75 billion a year market. The U.S. market is roughly 1/10 of the world market and Figure 22 provides a useful breakdown of the U.S. consumption of the different stainless steel product lines.

Specialty Steel Product Lines	U.S. Consumption	
	2004	Increase/Decrease 04 vs. 03
Stainless Sheet/Strip	1,811,334	14%
Stainless Plate	288,035	2%
Stainless Bar	204,638	11%
Stainless Rod	73,641	16%
Stainless Wire	81,707	13%
<b>Total Stainless Steel</b> (Sheet, Strip, Plate, Bar, Rod & Wire)	<b>2,459,356</b>	<b>13%</b>

**Figure 22. Breakdown of 2004 U.S. stainless steel consumption in short tons.**

Even though stainless steels are used in many industries because of their resistance to corrosion and reasonable price, they can still be prone to failure. In 1997, the Materials Technology Institute (MTI) of the Chemical Process Industries, Inc., published a compilation of experiences of corrosion failure mechanisms in several process industries that showed cracking and intergranular corrosion (included in local attack) to be the two of the most common failures (Figure 20) [29]. Figure 21 also illustrates findings from the study showing stainless steels were involved in a majority of these failures.

FAILURE MODE	AVERAGE FREQUENCY (%)
Cracking	36
General Corrosion	26
Local Attack	20
Temperature Effects	7
Velocity Effects	5
Voltage Effects*	3
Hydrogen Effects	2
Biological	0
<b>TOTAL</b>	<b>99%</b>

MATERIAL	AVERAGE FREQUENCY (%)
Stainless Steels	61.4
Steel	30.4
Copper Alloys	4.3
Nickel Alloys	2.8
Titanium	0.7
Tantalum	0.3
<b>TOTAL</b>	<b>99.9%</b>

**Figures 20 and 21. Failure mode and material frequency in process industry equipment [29].**

Process industries including chemical, petrochemical, and pharmaceutical spend an estimated \$1.7 billion per year on corrosion prevention [29]. Grain boundary engineered stainless could be particularly useful in such a market because of they are 2 – 10 times more resistant to intergranular failures such as cracking or corrosion.

Intergranular attack is also a major problem for electrical utilities with nuclear power plants. At Oconee Nuclear Station in 1998, nearly \$20 million was spent replacing steam generators and tubing because of intergranular attack [29]. Many more (>40) PWR reactors experience the same problem and cost every year. As the nuclear industry continues to produce nuclear waste, the challenge to find a safe storage mechanism for it is becoming even greater. Grain boundary engineered materials could take a central role in this growing market where material lifetimes are needed to reach for 10,000 years.

### 3.2 Competition

Grain boundary engineering improves materials' resistance to corrosion, cracking, and intergranular attack. As mentioned before, grain boundary engineered materials' chief competition in the market will be higher-grade stainless steels, specialty nickel-alloys or superalloys. In any case, these markets are dominated by the large steel producers of the world and on down through the major domestic markets. The world market consists of one or two major players in each large industrialized country or region. These include Nisshin Steel Corp. (Japan), Thyssen Krupp (Italy), Outokumpu Stainless (Finland), United Steel Corp. (Taiwan), Acerinox (Spain) and Taiyun (China). Taiyun recently announced an expansion of capacity from 1.5 million tons to 3 million tons by 2006, which would make them the largest producer in the world. The major steel producers such as Allegheny Ludlum, North American Stainless, AK Steel, and Universal Stainless & Alloy Products also dominate the United States market. If a new company were to be formed to produce grain boundary engineered products, it likely would be necessary to focus on a particular niche product at the start in order to establish a foothold in the marketplace. Another option could be exclusive or non-exclusive licensing partnerships with some of these large existing steel producers.

There is also an existing company producing grain boundary engineered materials. Integran Technologies, Inc. was spun off from Ontario Hydro in Canada and is managed by several of the first grain boundary engineering researchers in the late 1980's and early 1990's including Dr. Gino Palumbo, Dr. Uwe Erb, Dr. Edward M. Lehockey, and Dr. Peter K. Lin. Integran's intellectual property (IP) holdings are extensive and include the trademark GBE® (grain boundary engineered) as well several other patents accounting for more than half of all existing grain boundary engineering IP. Integran's description of their GBE® technology from [www.integran.com](http://www.integran.com) states:

“Via patent-protected thermomechanical processes (forming & heat treatment), the internal structure of conventional metals and alloys is optimized locally on a nanometer scale to yield breakthrough improvements in material reliability, durability and longevity.”

Integran's GBE® process can be applied to components during the forming/finishing process or as a surface treatment (0.1 to 1mm case depth) to finished or semi-finished components. They have targeted several products including copper shaped charge liners, combustion turbine engine components, lead acid battery electrodes, nuclear reactor and fossil plant components and nuclear waste containment. A new company created to compete with Integran would need to develop strong IP to either trump or circumvent their existing IP as discussed in the previous chapter. This new company would also need niche applications to focus on or much more competitive pricing than Integran.

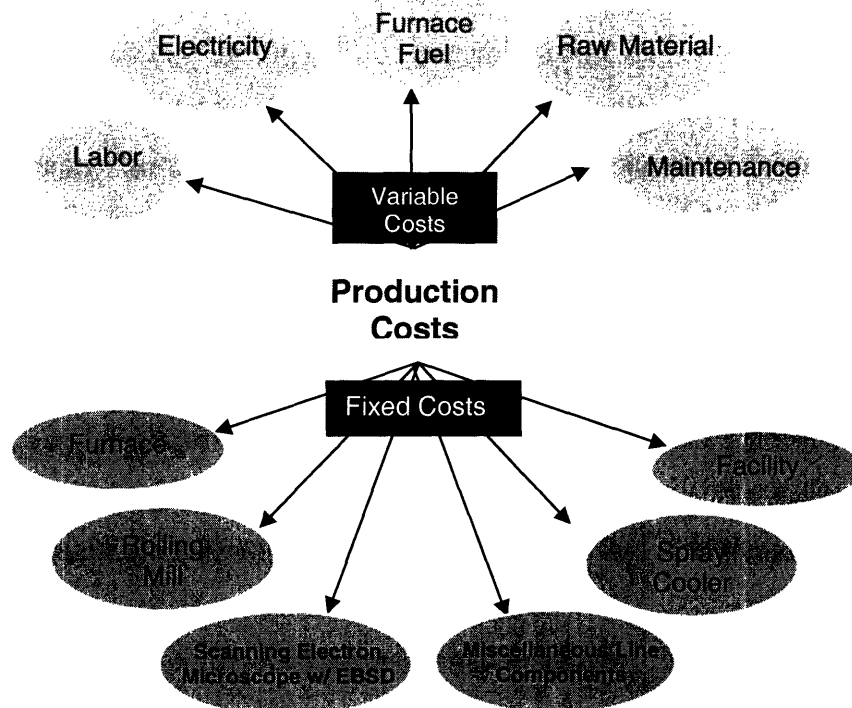
### 3.3 Cost Analysis

Entry into a market with a new product requires fulfillment of one or both of two basic categories:

- Enter an existing market with a superior product produced to compete cost effectively with the competition
- Reduce the cost of an existing product with a similarly performing product

Grain boundary engineering technology would be entering the specialty metal alloy market with a superior technology; however, it must be shown as cost effective in order to succeed.

The cost analysis is based on the continuous production of type 304 stainless steel sheet described in the processing analysis section and detailed with calculations in Appendix A. It is only meant to provide a first look at the costs to speculate which product areas grain boundary engineered materials could possibly enter.



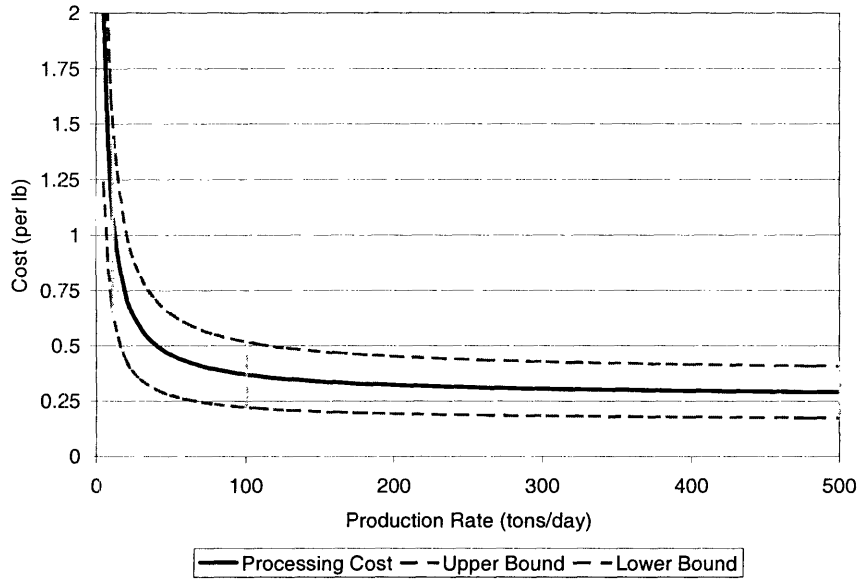
**Figure 23. Schematic of costs for the continuous production of sheet metal.**

Figure 23 illustrates the fixed and variable costs associated with the continuous production of sheet metal. The fixed costs represent all capital costs required for setting up a new production line for grain boundary engineering stainless steel sheet. The furnace is by far the most expensive piece of equipment. Correspondence with engineers at Furnace and Combustion Engineers (FCE) estimated its cost in the range of 10's of millions of dollars depending on the length and several other variables. Therefore, the furnace was estimated to cost \$3 million per 100 meters of travel but conservatively bracketed between \$1 million on the low end and \$5 million on the high end to provide

an upper and lower bound to the costs. This should be conservative enough to include additional expenses such as a protective gaseous environment of hydrogen, argon, nitrogen, etc. Other budgeted costs (with low and high ranges in parentheses) include: \$4 million for a rolling mill (\$1 million – \$10 million), \$50,000 for a sheet cooler (\$10,000 – \$100,000), \$150,000 for an scanning electron microscope with electron backscatter diffraction capabilities (\$100,000 - \$200,000), \$2 million for a facility (\$1 million - \$5 million) and \$500,000 for other miscellaneous line equipment (\$100,000 - \$1,000,000). Miscellaneous line equipment is meant to include all manner of coilers, bridles, and tension devices for driving, spooling, and controlling the sheet. Every additional process cycle was assumed to require an additional set of equipment to accomplish it, making a dual cycle process twice as expensive as a single cycle process. Capital costs were divided into yearly payments assuming 10 years of payments with an interest rate of 10%.

The major variable costs include electricity to run the rolling mill, line components and spray cooler and fuel for heating the annealing furnace. Electricity was assumed to cost \$0.06 per kW-h. The annealing furnace was assumed to burn natural gas at \$0.60 per therm. Labor was assumed to be provided by 5 workers making \$20 per hour (2 – 10 workers) and maintenance costs were estimated at \$100,000 a year (\$50,000 - \$500,000).

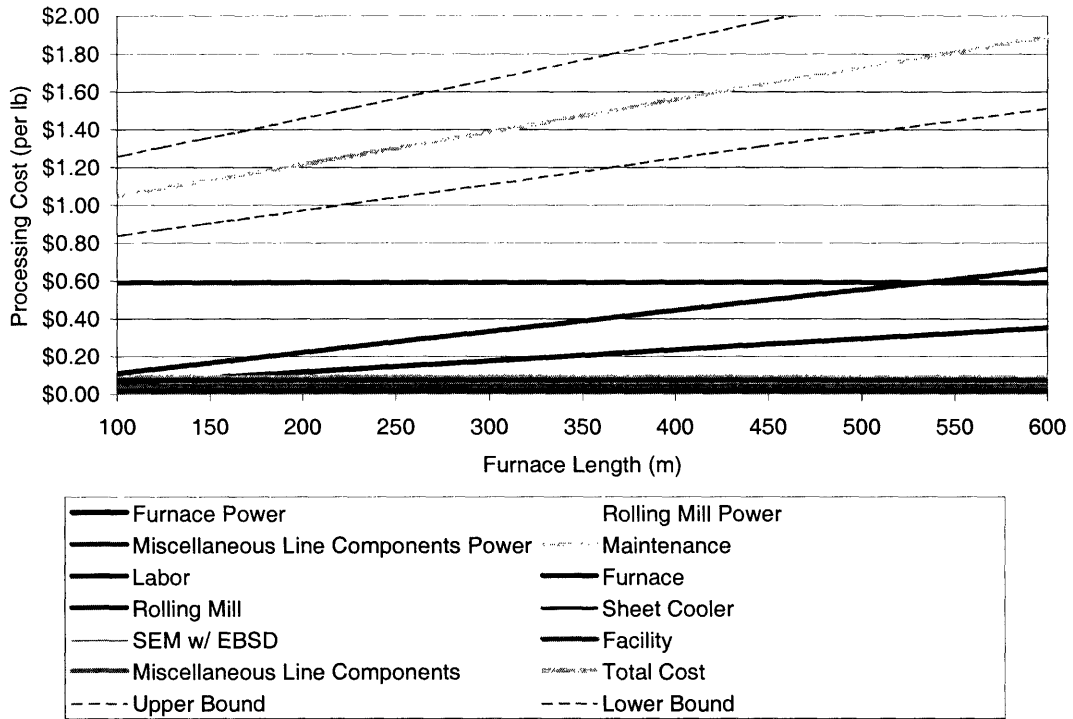
Figure 24 shows the total processing cost for the benchmark processing conditions vs. production rate along with an estimated upper and lower bound. If a new company were created to produce grain boundary engineered materials, production rates would likely be in the 10 – 50 tons per day or about 2000 – 10,000 tons per year. These rates would place the total processing cost in the \$1 - \$2 per lb range if modest production rates of 10 tons/day (or ~2200 tons year) were expected but could drop to \$0.40 to \$0.70 per if production was as high as 50 tons/day. If a large market could be found to push production rates higher or if a partnership was entered into with a large, established manufacturer, increasing production rates could take further advantage of the associated economies of scale, possibly pushing costs into the \$0.20 - \$0.40 range.



**Figure 24. Total processing cost with upper and lower bounds for the benchmark processing conditions.**

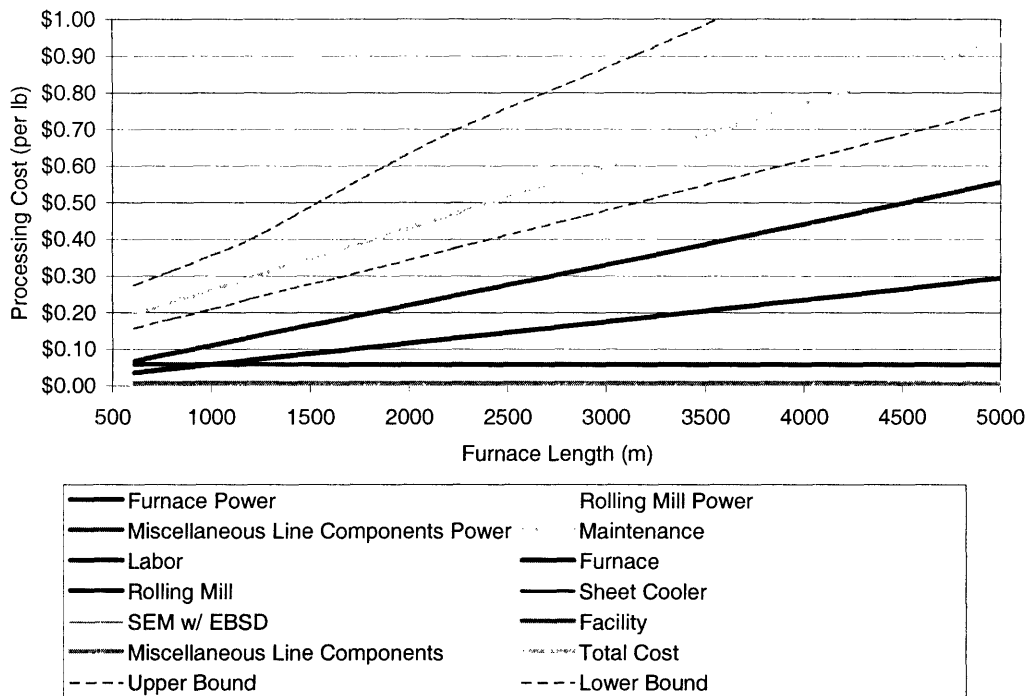
The largest factor driving up the cost of a line is the length of the furnace necessary. This is because the increasing length requires more radiant silicon/silicon carbide tubes to heat and anneal the sheet, increasing the capital cost and burning more fuel. As shown in the previous section, many of the processing variables affect the length. The number of cycles, annealing time, annealing temperature, and production rate all cause the furnace length to increase as they increase. Only increasing the amount of strain per cycle leads to a slight decrease in the length of the furnace. Therefore, by estimating the approximate length of a line required for a particular production rate, the cost per lb of a grain boundary engineering process can also be estimated.

Figure 25 shows the various costs per lb as contributed by each of the fixed and variable costs of the process for a production rate of 10 tons/day. As shown in the earlier section, at this production rate furnace lengths should reside in the 100 – 600 m range putting the cost per pound in the \$1 – \$2 range.



**Figure 25. Processing Costs per lb vs. Furnace Length for a 10 ton/day production rate.**

For very short furnace lengths, the rolling mill is the dominant cost. However, it is overtaken by the furnace and furnace power costs as the furnace length exceeds 500 m and enters the 1000's of meters as shown in figure 26.



**Figure 26. Processing Costs per lb vs. Furnace Length for a 100 ton/day production rate.**

In either case, the benchmark grain boundary engineering process appears to cost a minimum of about \$0.20 - \$0.40 per lb to accomplish. However, more cycles, a longer annealing time, greater annealing temperature, or lower production rate could increase this cost nearer to \$1 - \$2 per lb. At the same time, if a grain boundary engineering process could be optimized such that less cycles, a shorter annealing time, or a lower annealing temperature could be discovered, costs would stay at the much more reasonable \$0.20 - \$0.40 per lb.

Commercialization of grain boundary engineering technology depends strongly upon the price the market would be willing to pay for the product. As mentioned in the section above, grain boundary engineering of a less expensive alloy such as type 304 could make it as resistant to intergranular degradations as a more expensive, higher-grade alloy such as type 316 that relies on the addition of more exotic elements for its resistance. For example, the price disparity between the cost of types 304 and 316 stainless steels has been rapidly increasing over the last several months as shown in Table 3 [74]. This trend

also likely exists for other stainless steel alloys and if continued, a significant margin exists for grain boundary engineered materials to enter the market and compete with the higher grades of alloys.

However, it is impossible to predict the exact materials or alloys grain boundary engineered materials will compete with or replace without further research. Published studies to this point have focused only on the improvement of the grain boundary engineered material's performance over that of the base material in the study. There is a lack of direct comparison between grain boundary engineered materials and higher-grade specialty alloys that would be a step up from the base material in question. Therefore, more examinations and comparisons will need to be completed to identify the specific applications and competition in the market. Further research must also be completed to understand the effect post-production joining processes will have on grain boundary engineered materials. Welding is one of the most common methods for accomplishing this, however, it is not understood how the heat input from the welding process will affect the grain boundary network that was so carefully crafted during the grain boundary engineering processing. Either way, grain boundary engineering is clearly a promising enough technology to continue investigating and should eventually become a very successful and competitive technology in the market.

	Cold Rolled Coil (\$/ton)		Price Difference (\$/lb)
	304	316	
May-03	1690	2314	\$0.31
Jun-03	1680	2309	\$0.31
Jul-03	1685	2331	\$0.32
Aug-03	1672	2312	\$0.32
Sep-03	1723	2361	\$0.32
Oct-03	1811	2491	\$0.34
Nov-03	1869	2584	\$0.36
Dec-03	1961	2688	\$0.36
Jan-04	2137	2919	\$0.39
Feb-04	2372	3222	\$0.43
Mar-04	2484	3399	\$0.46
Apr-04	2509	3409	\$0.45
May-04	2532	3463	\$0.47
Jun-04	2478	3574	\$0.55
Jul-04	2405	3561	\$0.58
Aug-04	2382	3527	\$0.57
Sep-04	2679	4014	\$0.67
Oct-04	2666	4106	\$0.72
Nov-04	2718	4240	\$0.76
Dec-04	2827	4502	\$0.84
Jan-05	2783	4619	\$0.92
Feb-05	2712	4736	\$1.01
Mar-05	2748	4877	\$1.06
Apr-05	2748	4794	\$1.02

**Table 3. Price disparity between type 304 and 316 stainless steels increasing recently [74].**

## **Conclusions**

In conclusion, grain boundary engineering will no doubt become a successful commercial technology. It has already been commercialized on a small scale by Integran Technologies Inc. and as demonstrated in this evaluation, it could effectively be scaled-up into a much larger scale production. Grain boundary engineered materials will likely enter specialty metal markets by improving lower grade FCC materials to perform equivalently with higher grade materials at a lower cost because they do not require expensive, exotic elements to be alloyed in. The barriers which must be overcome in order to reach larger scale commercial success include (i) the demonstration of equivalent performance to more expensive, higher grade alloys while keeping production costs low, and (ii) demonstration of welding and joining technologies in finished products that will not undo the carefully crafted grain boundary engineered microstructure. Commercialization will also require the acquisition of grain boundary engineering intellectual property either through the development and patent of new processes or through the licensing of protected processes. Current work on grain boundary engineering effectiveness parameters might lead to the development of new IP, however, due to possible similarities between these new parameters and those in current use, litigation may be brought about upon filing of the new IP. With successful IP, small or large scale productions are possible depending on the forecasted demand of the envisioned product as well as licensing options with an established producer to minimize capital costs and take advantage of the economies of scale. Finally, grain boundary engineering is still in an embryonic stage and its complete potential is still very much untapped. It could also improve and push the boundaries of even the highest performance materials in many varying fields. However, initial commercialization will still require further research on post-production effects and specific environmental performance and limitations before exact products and applications can be identified with certainty.

## References

- [1] Watanabe T. Res. Mech 1984;11:47.
- [2] Watanabe T, Tsurekawa S. J. Mater. Sci. 2005; 40: 817.
- [3] C. Schuh. Unpublished images.
- [4] Gourgues A-F, Mat. Sci. Technol. 2002; 18: 119.
- [5] Brandon DG. Acta metal 1966;14:1479.
- [6] Palumbo G, Aust KT. Acta Metal. 1990; 28: 2343.
- [7] Palumbo, G. and K.T. Aust, *Special Properties of Sigma Grain Boundaries*, in *Materials Interfaces*, D. Wolf and S. Yip, Editors. 1992, Chapman and Hall: London. p. 190-211.
- [8] Trillo EA, Murr LE. Acta Mater. 1999; 47: 235.
- [9] Bi HY, Kokawa H, Wang ZJ, Shimada M, Sato YS. Scripta Mater. 2003; 49: 223.
- [10] Zhou Y, Aust KT, Erb U, Palumbo G. Scripta Mater. 2001; 45: 49.
- [11] Aust KT, Erb U, Palumbo G. Mater. Sci. Eng. 1994; A176: 333.
- [12] Lehockey EM, Palumbo G, Lin P, Brennenstuhl A. Metall. Mater. Trans. 1998; 29A: 387.
- [13] Palumbo G, Aust KT. Acta Metall. Mater., 1990; 38: 2343.
- [14] Shimada M, Kokawa H, Wang ZJ, Sato YS, Karibe I. Acta Mater 2002;50:2337.
- [15] Lin P, Palumbo G, Erb U, Aust KT. Scripta Metall. Mater. 1995; 33: 1387.
- [16] Crawford DC, Was GS. Metall. Trans., 1992, 23A, 1195.
- [17] Pan Y, Adams BL, Olson T, Panayotou N. Acta Mater. 1996; 44: 4685.
- [18] Gertsman VY, Bruemmer SM. Acta Mater. 2001; 49: 1589.
- [19] Lehockey EM, Palumbo G, Lin P. Scripta Mater. 1998; 39: 353.
- [20] Alexandreanu B, Sencer B, Thaveprungsriporn V, Was G. Acta Mater. 2003; 51: 3832.
- [21] Thaveprungsriporn V, Was GS. Metall. Trans. 1997; 28A: 2101.
- [22] Lehockey EM, Palumbo G. Mater. Sci. Eng. 1997; A237:169.
- [23] Watanabe T. Mater. Sci. Eng. A176, 39.
- [24] Schuh CA, Kumar M, King WE. Acta Mater. 2003; 51: 687.
- [25] Palumbo G, King PJ, Aust KT, Erb U, Lichtenberger PC. Scripta Metall. 25 (1991) 1775.
- [26] Lehockey EM, Brennenstuhl AM, Thompson I. Corr. Sci. 46 (2004) 2386.
- [27] Mahajan S, Pande CS, Imam MA, Rath BB. Acta Mater. 1997; 45: 2634.
- [28] Frary M, Schuh CA. Physical Review B. 2004; 69; 134115-5.
- [29] G. H. Koch, M. P. Brongers, N. G. Thompson, Y. P. Virmani, J. H. Payer. "Corrosion Cost and Preventative Strategies in the United States." FHWA-RD-01-156, Federal Highway Administration, 2001.
- [30] S. Kalpakjian and S. Schmid. "Manufacturing Processes for Engineering Materials." Prentice Hall, Upper Saddle River, NJ, 2003.
- [31] Randle V. Acta Mater. 2004;52:4067.
- [32] Thaveprungsriporn V, Sinsrok P, Thong-Aram D. Scripta Mater. 2001; 44: 68.
- [33] King WE, Schwartz AJ. Scripta Mater. 1998; 38: 450.
- [34] Lee SL, Richards NL. Mater. Sci. Eng. 2005; A390: 85.
- [35] Davies H, Randle V. Mater. Sci. Tech. 2000; 390: 1400.
- [36] Alexandreanu B, Capell B, Was GS. Mater. Sci. Eng. 2001; A300: 94.

- [37] Thomson CB, Randle V. *Acta Mater.* 1997; 45: 4911.
- [38] Schwartz AJ, King WE. *JOM* 1998; Feb; 54.
- [39] Kumar M, King WE, Schwartz AJ. *Acta Mater.* 2000; 48: 2081.
- [40] Schwartz AJ, Kumar M, King WE. *Proceedings of the Materials Research Society, Symposium on Interfacial Engineering for Optimized Properties II.* 2000; 586: 3.
- [41] Palumbo, Gino. Metal alloys having improved resistance to intergranular stress corrosion cracking. Integran Technologies, assignee. Patent 5,817,193. 06 Oct. 1998.
- [42] Krupp U, Kane WM, Liu X, Dueber O, Laird C, McMahon CJ. *Mater Sci Eng A* 2003; 349: 215.
- [43] Guyot BM, Richards NL. *Mat Sci Eng A.* 2005; 395: 96.
- [44] Randle V, Davies H. *Met Mater Trans A* 2002; 33: 1853.
- [45] Lee DS, Ryoo HS, Hwang SK. *Mater Sci Eng A* 2003; 354: 106.
- [46] Qian M, Lippold JC. *Acta Mater* 2003;51:3351.
- [47] Randle V. *Acta Mater* 1999;47:4187.
- [48] J. N. Harris. "Mechanical Working of Metals", Pergamon Press, New York, NY, 1983.
- [49] G. J. Richardson, D. N. Hawkins, C. M. Sellars. "Worked Examples in Metalworking", The Institute of Metals, London, 1985.
- [50] W. Roberts. "Flat Processing of Steel." Marcel Dekker, Inc, New York, NY, 1988.
- [51] A. Milani and J. G. Wüning. "Radiant Tube Technology for Strip Line Furnaces." *IFRF Combustion Journal.* 200405, 2004.
- [52] J. R. Howell. "A Catalog of Radiation Configuration Factors." McGraw-Hill Book Co., New York, NY, 1982.
- [53] D. R. Poirier and G. H. Geiger. "Transport Phenomena in Materials Processing." The Minerals, Metals, and Materials Society, Warrendale, PA, 1994.
- [54] H. K. Kuiken. *Pro. R. Soc. Lond. A.* **341**, 233-252 (1974).
- [55] M. V. Karwe and Y. Jaluria. *ASME Journal of Heat Transfer.* **108**, 728-733 (1986).
- [56] M. V. Karwe and Y. Jaluria. *ASME Journal of Heat Transfer.* **110**, 655-661 (1988).
- [57] M. V. Karwe and Y. Jaluria. *Int. J. Heat Mass Transfer.* **35**, 493-510 (1992).
- [58] C. H. Chen. **36**, 79-86 (2000).
- [59] F. R. Incropera and D. DeWitt. "Introduction to Heat Transfer." John Wiley & Sons, Inc., New York, NY, 2002.
- [60] F. K. Tsou, E. M. Sparrow and E. F. Kurtz. *J. Fluid Mechanics.* **26**(1), 145-161 (1966).
- [61] S. W. Haplern, C. A. Nard, and K. L. Port. "Fundamentals of United States Intellectual Property Law." Kluwer Law International, Boston, 1999.
- [62] [http://www.ssina.com/news/releases/pdf\\_releases/7\\_08\\_05.pdf](http://www.ssina.com/news/releases/pdf_releases/7_08_05.pdf)
- [63] Hirasawa J, Furukimi O, Konakawa H, Shimada M, Yutaka S. Austenitic Stainless Steel Excellen in Intergranular Corrosion Resistance and Production Method Thereof. JFE Steel KK and Konakawa H, applicants. Patent JP2003253401. 10 Sep. 2003.
- [64] Kanzaki M, Amagasaki-shi. Nickel Alloy and Manufacturing Method for the Same. United States Patent Application Pub. No. US 2004/0156738 A1 12 Aug. 2004.
- [65] Lehockey E, Palumbo G, Lin P, Limoges D. Metallurgical Method for Processing Nickel- and Iron-Based Superalloys. Integran Technologies, assignee. Patent 6,129,795. 10 Oct. 2000.

- [66] Limoges D, Palumbo G, Lin P. Surface Treatment of Austenitic Ni-Fe-Cr-based Alloys for Improved Resistance to Intergranular-Corrosion and -Cracking. Integran Technologies, assignee. Patent 6,344,097. 5 Feb. 2002.
- [67] Riege SP, Prybyla JA, Hunt AW. Appl. Phys. Lett. 1996; 69: 2367.
- [68] Bika D, McMahon CJ, Jr. Acta Metall. Mater. 1995; 43: 1909.
- [69] Argon AS, Qiao Y. Phil. Mag. 2002; A82: 3333.
- [70] Van Swygenhoven H, Caro A, Farkas D. Scripta Mater. 2001; 44: 1513.
- [71] Xin G. Solid State Ionics 1995; 81: 235.
- [72] Hilgenkamp H, Mannhart J. Rev. Mod. Phys. 2002; 74: 485.
- [73] Moll, M. Steel Time International. 2004; June: 24.
- [74] <http://www.meps.co.uk/index-price.htm>
- [75] Metals Handbook Ninth Edition. Volume 3 Properties and Selection: Stainless Steels, Tool Materials and Special Purpose Metals. American Society for Metals, Metals Park, OH, 1980.
- [76] Palumbo G, Lehockey EM, Lin P. JOM. 1998; 50: 40.
- [77] Randle, V. Int. Mater. Rev. 2004; 49: 1.
- [78] Pan, Y., T. Olson, and B.L. Adams, *Applications of Orientation Imaging Analysis to Microstructural Control of Intergranular Stress Corrosion Cracking*. Canadian Metallurgical Quarterly, 1995. **34**: p. 147-154.
- [79] Gertsman, V.Y. and K. Tangri, *Modelling of Intergranular Damage Propagation*. Acta Materialia, 1997. **45**: p. 4107-4116.
- [80] Wells, D.B., et al., *The Use of Percolation Theory to Predict the Probability of Failure of Sensitized, Austenitic Stainless Steels by Intergranular Stress Corrosion Cracking*. Corrosion, 1989. **45**(8): p. 649-660.
- [81] Frary, M. and Schuh, C.A. *Modeling and Simulation of the Percolation Problem in High- $T_c$  Superconductors: Role of Crystallographic Constraints on Grain Boundary Connectivity*. Mat. Res. Soc. Symp. Proc. Vol. 819, 2004.
- [82] Gould, H. and J. Tobochnik, *An Introduction to Computer Simulation Methods*. 1996, Reading, MA: Addison-Wesley Publishing Company.
- [83] Stauffer, D., *Scaling theory of percolation clusters*. Physics Reports, 1979. **54**(1): p. 1-74.
- [84] Voss, R.F., R.B. Laibowitz, and E.I. Alessandrini, *Fractal (scaling) clusters in thin gold films near the percolation threshold*. Physical Review Letters, 1982. **49**(19): p. 1441-4.
- [85] Wolf D. Atomic-level geometry of crystalline interfaces. In: Wolf K, Yip S. editors. Materials interfaces atomic-level structure and properties. London: Chapman & Hall; 1992. p. 1.
- [86] Watanabe, T. Mater. Sci. Eng. A 1993, 166: 11.
- [87] Randle, V., *Mechanism of Twinning Induced Grain Boundary Engineering in Low-Stacking-Fault Energy Materials*. Acta Materialia, 1999. **47**: p. 4187-4196.
- [88] Lejcek P, Hofmann S, Paidar V. *Solute segregation and classification of [100] tilt grain boundaries in  $\alpha$ -iron: consequences for grain boundary engineering*. Acta Materialia, 2003. **51**: p. 3951-3963.
- [89] D. A. Jones. "Principles and Prevention of Corrosion", Prentice Hall, Upper Saddle River, NJ, 1996.



## Appendix A: Derivation of Rolling Process Equations

### A.1 Rolling

Rolling is the process of reducing the thickness of a long workpiece by compressive forces applied through a set of rollers to produce metal sheet or plate. It accounts for nearly 90% of all metals produced by metalworking processes and is used to turn out plates (6 – 300 mm thick) or sheets (< 6 mm thick). In order to assess the possible process schedules for GBE, the limits of production (maximum reduction per roll, rolling load and power required, etc.) must be considered. These limits will be calculated and discussed in the following section after the rolling process is explained.

The figure below shows a schematic of the rolling process. The rollers turn pulling the metal through the gap to the right. The metal's initial thickness of  $h_0$  is reduced to  $h_f$  after moving through the gap for a total reduction of  $\Delta h = h_0 - h_f$ . The rollers have equal radii of  $R$  and the pressure on the workpiece acts radially. There is only one point where the rollers and metal are traveling at the same speed that is called the Neutral Point as well as the Point of No Slip. For the area of contact from the point of entry to the neutral point, the rollers are traveling faster than the metal, thus dragging it into the gap. For the area of contact after the neutral point to the exit, the rollers are traveling more slowly than the material, thus resisting the movement through the gap.

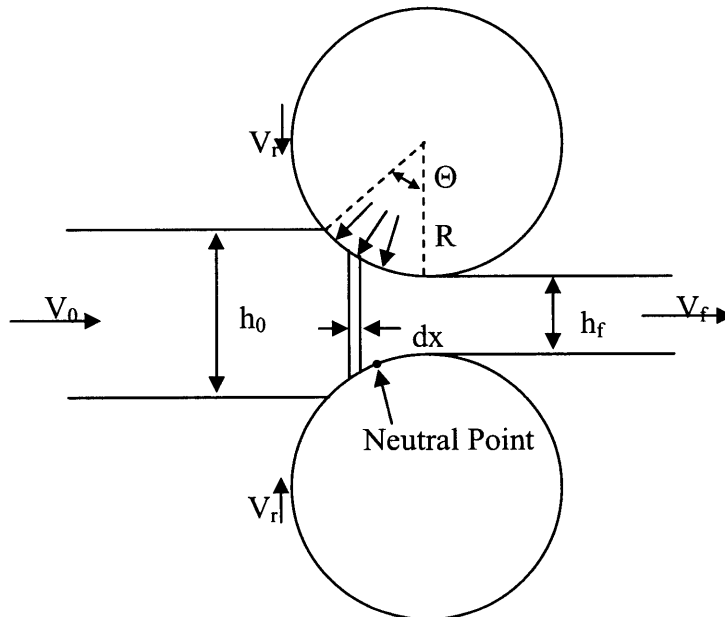


Figure 1A. Sheet metal rolling schematic.

### *A.1.1 Rolling speed*

The velocity at which the sheet moves through the rollers is an important process variable. This can be determined quite simply using the conservation of volume. Since rolling is assumed to change only the thickness of the sheet, the conservation equation reduces to:

$$V_i h_i = V_o h_o.$$

Thus for a deformation of 10%, the sheet speed upon exit will have increased by a factor of 1.11.

### *A.1.2 Friction*

Another important process variable in rolling is the amount of reduction in the thickness of the sheet. The amount of reduction possible is completely dependent on the coefficient of friction between the rollers and the metal sheet. The forces and power requirements also rise as the coefficient of friction increases. Therefore, the coefficient of friction is a very relevant physical control parameter in the rolling process.

Friction in cold rolling is largely dependent on the material being cold worked and the material type of the rollers. It will typically range from 0.02 – 0.3 during cold rolling [30] and can be decreased through the use of lubricants or increased by roughening the surface or the sheet or the rollers.

### *A.1.3 Rolling Reduction*

If you consider the element of length  $dx$  located between the point of entry and the neutral point from the figure above, you can see the forces acting on it due to friction and the radial pressure as shown in Figure 2A. The friction force acts to pull the metal into the rollers while the radial pressure from the rollers acts as an opposing force.

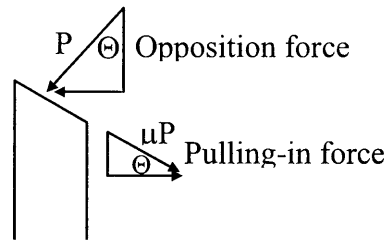


**Figure 2A. Horizontal forces acting on an element dx.**

Summing the horizontal forces results in  $\mu P \cos \Theta - P \sin \Theta$  and thus there exists a maximum angle possible for material entering the rollers before the opposition force exceeds the pulling-in force,

$$\mu P \cos \Theta_{\max} - P \sin \Theta = 0$$

or through simplification,

$$\mu = \tan \Theta_{\max}$$

Thus  $\Theta_{\max}$ , the maximum angle of bite of the rollers, is dependent only upon the coefficient of friction between the material and the rollers. The maximum possible reduction thus depends on  $\Theta_{\max}$  and this relationship can be derived using trigonometry as shown in Figure 3A to get:

$$\sin \Theta_{\max} = \frac{(R\Delta h)^{1/2}}{R}$$

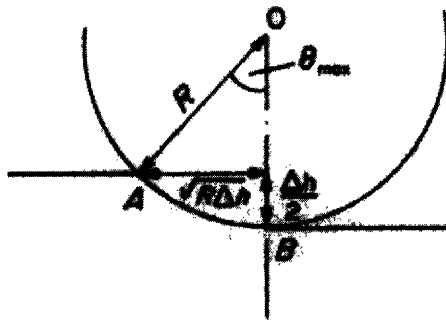


**Figure 3A. Schematic of single roller dimensions [48].**

Figure 4A is a plot of  $\Theta_{\max}$  vs. horizontal force showing that  $\Theta_{\max} \approx 6^\circ$  when the force is calculated assuming a coefficient of friction,  $\mu = 0.1$ . Since grain boundary engineering

could be performed on iron-, copper-, or nickel-alloys but at cold working temperatures, the coefficient of friction could possibly vary from 0.02 – 0.3. Figure 5A is a plot of Coefficient of friction vs. maximum reduction in mm for a pair of rollers with radii of 0.25 m showing that a coefficient of friction of 0.1 allows for a reduction  $\approx 2.4$  mm per roll. Assuming a possible coefficient range from 0.02 – 0.3 gives maximum reductions per roll of 0.02 – 21 mm respectively.

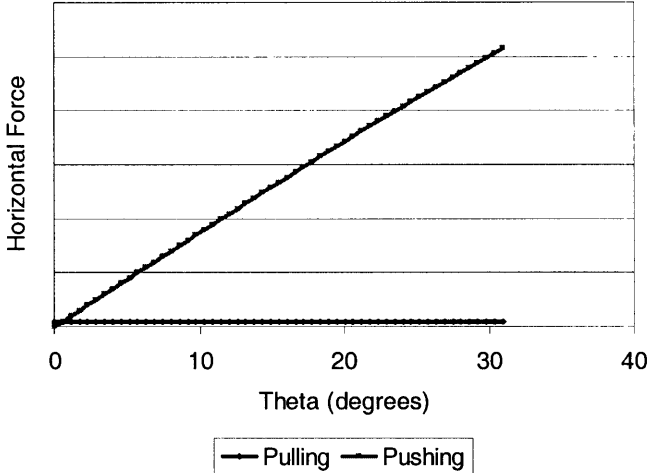


Figure 4A.  $\Theta_{max}$  vs. horizontal force showing  $\Theta_{max} \approx 6^\circ$  when  $\mu = 0.1$ .

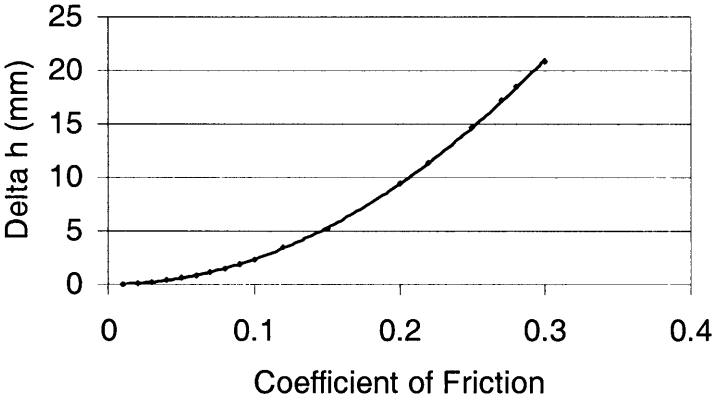


Figure 5A. Coefficient of friction,  $\mu$ , vs. maximum reduction,  $\Delta h$ .

*A.1.4 Estimate of Rolling Load*

The rolling load deforming the metal is equal to the stress H area of contact between the metal and the rolls. The stress, shown by the arrows in Figure 6A, acts radially and can be assumed to have a mean value of  $P_m$ . If the mean width of the metal in the rollers is

$W_m$  and the area of contact is the segment AB as shown in the figure, the roll load becomes:

$$RollLoad = P_m \cdot W_m \cdot AB$$

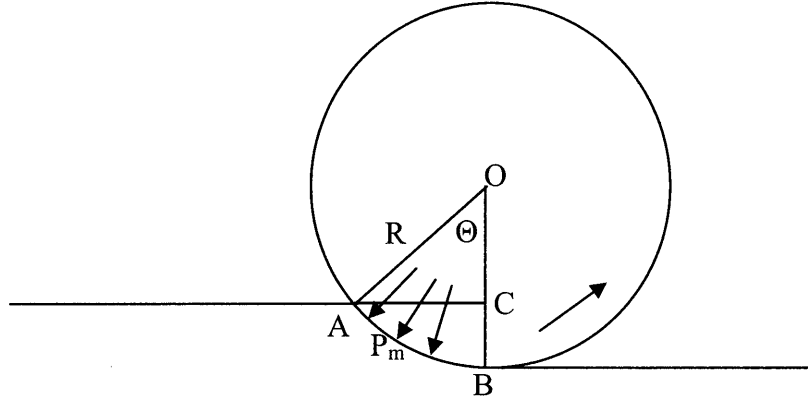


**Figure 6A. Single roller schematic.**

Thus, we must calculate the arc of contact between the rollers and the sheet. Using the Figure 6A we have:

$$\cos \Theta = \frac{OC}{OA} = R - \frac{\left(\frac{\Delta h}{2}\right)}{R}$$

and

$$AB = R\Theta = R \cos^{-1} \left( 1 - \frac{\Delta h}{2R} \right).$$

The roll load equation above requires the assumption that the width of the material remains constant. During rolling, the friction between the metal and the rollers tends to stop the material from sliding axially across them and the width of the metal before rolling also tends to prevent spreading if the ratio of the width to the arc of contact,  $(R\Delta h)^{1/2}$ , is greater than 5 to 1. When this ratio is exceeded, the deformation can be considered plane strain and the width remains substantially constant. However, the homogenous yield stress is not the criterion of yielding and the Von Mises criterion must be used [48] where yielding in plane strain occurs at  $1.155 \sigma_0$ . Thus, the assumptions and subsequent simplifications make the equation:

$$RollLoad = 1.155\sigma_0 W_m R \cos^{-1}\left(1 - \frac{\Delta h}{2R}\right)$$

#### *A.1.5 Roll Flattening*

Once the roll load has been estimated, the roller radius can be corrected for elastic deformation in the rollers. Even though rollers will exhibit high levels of hardness and no tendency towards plastic deformation, they will still react a small, finite amount elastically such that the radius of curvature of the arc of contact is increased. The best-known formula for calculating this deflection was proposed by Hitchcock [48]:

$$R' = R\left(1 + \frac{CP'}{W\Delta h}\right)$$

where

$$C = 16 \frac{(1 - \gamma^2)}{\pi E}$$

where  $\gamma$  = Poisson's ratio, E is Young's Modulus, and P' is the rolling load based on the radius R'. Thus, iteration is necessary until R' converges.

#### *A.1.6 Roll Pressure*

The simplified approach presented earlier was necessary to be able to adjust the more accurate calculation of rolling load for elastic deformation and roll flattening. Therefore, each of the rolling load and roll flattening can be iterated using each other's improved calculations to improve the final calculation. This calculation of rolling load takes into account the fact that the metal moves and gradually decreases in thickness, factors that were ignored in the original estimation. Orowan developed the most accurate theory but a far simpler theory by Bland and Ford loses little accuracy and will be used here. The following assumptions are necessary, some of which have already been stated [48]:

1. Plane strain deformation conditions operate.
2. No shear occurs in vertical planes, i.e. homogeneous deformation.
3. Neutral point falls within the arc of contact.
4. Coefficient of friction is constant.
5. Circular arc of contact.
6. Elastic deformation is negligible.
7. Principle stresses are  $\sigma_1 = \sigma_x$  and  $\sigma_3 = -P$ .
8. Tresca's Yield criterion holds, i.e.  $\sigma_1 - \sigma_3 = 1.155 \sigma_0$ .

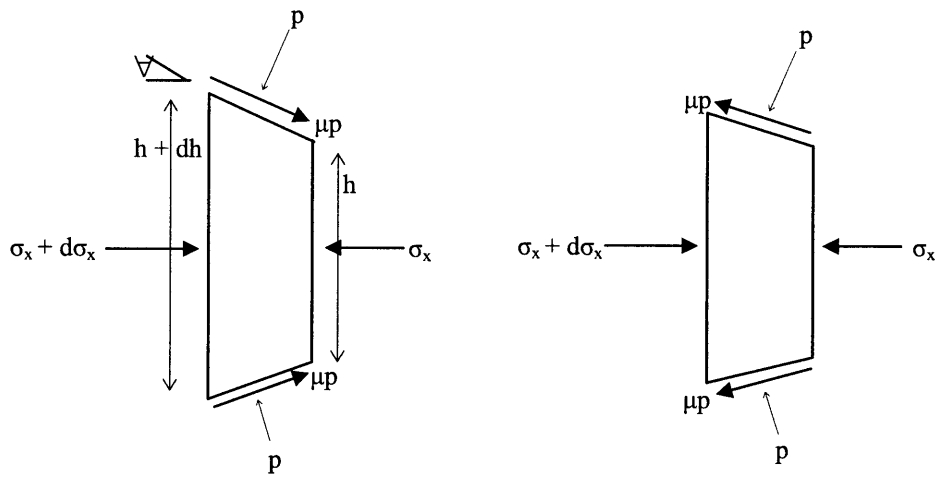


**Figure 7A. Forces on sheet elements before and after rolling reduction.**

The roll pressure distribution can be calculated using the slab method of analysis for plane strain and the derivation of Kalpakjian and Schmid [30] produces the equations for the pressure on the entrance and exiting sides of the neutral point:

$$P_{entry} = Y'_f \frac{h}{h_0} e^{\mu(H_0 - H)}$$

and

$$P_{exit} = Y'_f \frac{h}{h_f} e^{\mu H}$$

The neutral point shown in Figure 1A exists where the rollers and the metal sheet are traveling at the same speed. At this point, the frictional force on the left or entry side of the neutral point must be greater than the force on the right or exit side, thus providing for a net force pulling the sheet into the rollers for subsequent deformation. Since the entry and exit zone pressures are equal at this point, it can be calculated by finding the angle,  $\Theta$ , where  $p_{\text{entry}} = p_{\text{exit}}$ .

#### A.1.7 Tensioning

An effective way of reducing the roll force is to apply tension to the front and back ends of the sheet. This reduces the apparent compressive yield stress by decreasing the yield stress normal to the sheet's surface. Therefore, the equations for entry and exit zone pressure are decreased by the front and back tension,  $\sigma_f$  and  $\sigma_b$ , respectively leading to:

$$p_{\text{entry}} = \left( Y_f - \sigma_b \right) \frac{h}{h_0} e^{\mu(H_0 - H)}$$

and

$$p_{\text{exit}} = \left( Y_f - \sigma_b \right) \frac{h}{h_f} e^{\mu H}.$$

Tension is a simple and effective way of decreasing the pressure on the rolls as well as decreasing the torque and power requirements. The coiler or delivery reel applies front tension and back tension is applied by the braking system in the uncoiler.

#### A.1.8 Rolling Force

The rolling force,  $F$ , can be calculated by integrating the equations for  $p_{\text{entry}}$  and  $p_{\text{exit}}$  over their respective arcs of contact:

$$F = \int_{\Theta_n}^{\Theta_n} w R p_{\text{entry}} d\Theta + \int_{\Theta_n}^{\Theta_n} w R p_{\text{exit}} d\Theta$$

### A.1.9 Roll Torque

The torque necessary to accomplish rolling can be calculated through determination of the turning moment applied to the roller necessary to produce the frictional force at the surface of the roller. The torque, T, for one roller is

$$T = \int_{\Theta_n}^{\Theta} w\mu RR' p_{entry} d\Theta - \int_{\Theta}^{\Theta_n} w\mu RR' p_{exit} d\Theta .$$

The equation includes the deformed roller radius, R', because the frictional forces act over the arc of contact 1R' and the undeformed roller radius, R, because it is turning moment lever arm [49]. The frictional force at the exit is opposite that at the entrance thus reducing the torque necessary to drive rolling.

### A.1.10 Roll Power

To calculate the power required per roller, start with Power = T\*T where T = 2BN and N is the number of revolutions per minute. By arranging terms as

$$Power = \frac{\pi TN}{30000} \text{ kw,}$$

the power can be calculated in terms of kW per roller.

## Appendix B: Derivation of Annealing Process Equations

The second important process in producing GBE materials is the annealing and heat treatment step. Annealing would be performed continuously with the sheet running through a furnace similar to Figure 1B from right to left. However, a GBE continuous annealing furnace would not need the cooling zones used for aging steels. After annealing for the required time, the sheet can be cooled immediately using arrays of air jets.

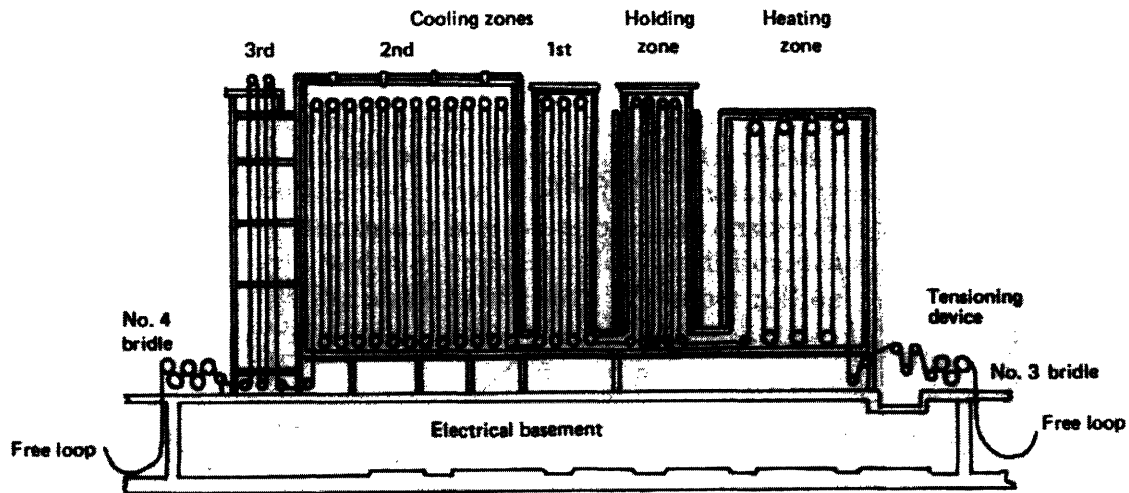


Figure 1B. Continuous annealing furnace [50].

### B.1 Radiant Heat Transfer

Continuous annealing furnaces primarily make use of radiant heat to pre-heat and anneal sheet metal. Radiant heat is supplied by radiant tubes such as that shown in Figure 2B.

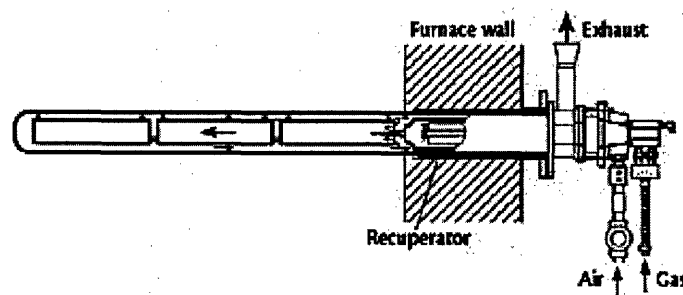
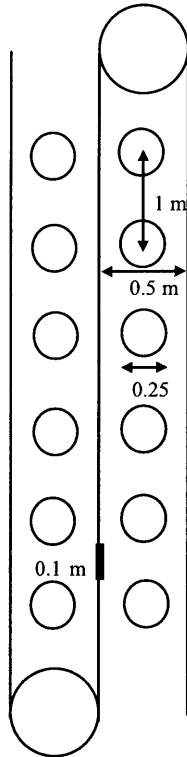


Figure 2B. Radiant tube for a continuous annealing furnace [51].

Radiant tubes made from silicon silicon-carbide (SiSiC) provide high heat fluxes approaching  $5,000,000 \text{ BTU/m}^2$  for temperatures up to  $\sim 1250^\circ\text{C}$  and emissivities of  $\sim 0.9$ . The tubes are about 50% efficient with no modifications but can reach as high as

90% when rechanneling the used flue gas to preheat the incoming combustion gas. Efficiency is also diminished by heat loss in the furnace to the walls, conveyor, and through the opening and exits. Therefore, the furnace will be conservatively assumed to be 25% efficient.



**Figure 3B. Model of sheet traveling in furnace past radiant tubes.**

The sheet travels through the furnace past the radiant tubes similar to the schematic in Figure 3B. The height of the furnace was assumed to be 8 m, however, this could ultimately depend on the tensile strength of the sheet and was assumed to be feasible. The tubes are evenly spaced 1 m apart so that as the sheet travels vertically up and down past them, it receives the radiant heat on both surfaces. At the top and bottom are drive rolls, however, heat conduction from them are neglected in this model. Heat can also be reradiated from the furnace walls to the lower temperature sheet but this is neglected in the model as well. The temperature change in the sheet is calculated by considering the amount of heat transferred into a 0.1 m section of the sheet as it travels through the furnace.

As it passes by each of the tubes, its view factor (and subsequent heat transfer) will change according to the equation shown in Figure 4B. Since the heat transfer was calculated for a 0.1 m segment of 1 m wide sheet,  $A_2 = 0.1 \text{ m}^2$ . Continuing through the other variables shown in Figure 4B, it was assumed that  $r = 0.25 \text{ m}$ ,  $a = 0.25 \text{ m}$ , and  $A_1 = 2\pi r h$  where  $h = 1 \text{ m}$  (the width of the sheet). Finally  $b_1$  and  $b_2$  were calculated for each 0.1 m segment sequentially along the

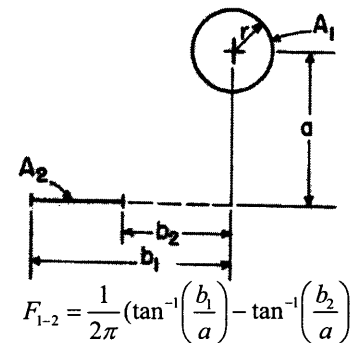


**Figure 4B. View factor equation and model for a small section traveling past a radiant tube [52].**

sheet assuming each tube can see segments a maximum of 2 m away. Therefore, each segment could possibly receive some fraction of transferred heat from 4 separate tubes at a time.

The heat transfer between the tubes and the sheet is assumed to occur between two gray bodies, thus assuming all radiation wavelengths are absorbed equally and the absorptivity is equal the emmissivity. The sheet was assumed to have an constant emmissivity of 0.3 while the tubes have a constant emmissivity of 0.9. Therefore, the view factor is used to calculate the total resistance of the analog circuit of the connected radiosity nodes shown in Figure 5B.

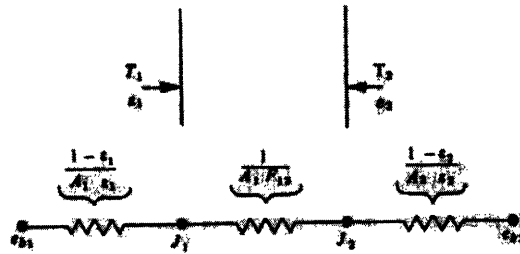


Figure 5B. Analog circuit representing heat transfer between surfaces [53].

The resistance of the circuit above is

$$\mathcal{F} = \frac{1}{\frac{1-\varepsilon_1}{A_1\varepsilon_1} + \frac{1}{A_1F_{12}} + \frac{1-\varepsilon_2}{A_2\varepsilon_2}}$$

where  $\varepsilon$  is the surface emmissivity,  $A$  is the surface area,  $F_{1-2}$  is the view factor and values were assumed as stated above. The radiant heat transfer to each segment is

$$q_{r,x} = \mathcal{F}_{12}\sigma(T_1^4 - T_2^4)$$

where  $T$  is the temperature of each respective surface and  $\sigma$  is Boltzmann's constant. The calculated heat transfer was finally multiplied by the length of the segment and divided by the sheet's velocity to calculate the amount of time the segments resided in the calculated view factor region. For example, a segment of 0.1 m moving at 1 m/s resided in a view factor zone for only 0.1 seconds and the calculated heat transferred for each

segment was adjusted by this value. In this way, the maximum calculated radiant heat transferred was ~1580 W for the lowest calculated sheet velocity of 0.1 m/s. Finally, the radiant heat transfer coefficient is

$$h_{r,x} = \frac{q_r}{(T_1 - T_2)}$$

The maximum radiant heat transfer coefficient was calculated to be ~15 W/m<sup>2</sup>\*K.

### *B.2 Convective heat transfer*

Heat transfer to the sheet traveling through the furnace also occurs by convective heat transfer. Several examinations have worked to analyze the thermal transport of a continuously moving sheet in a quiescent medium [54-58] but a good approximation to these cases is the case of forced convection with parallel flow over a stationary, flat plate (Blasius flow). The velocity of the sheet moving through quiescent air is assumed to be equal to velocity of the air flowing over the stationary flat plate. Fluid flowing over a flat plate experiences a transition in flow type from laminar to turbulent at some length L along the sheet as shown in Figure 6B.

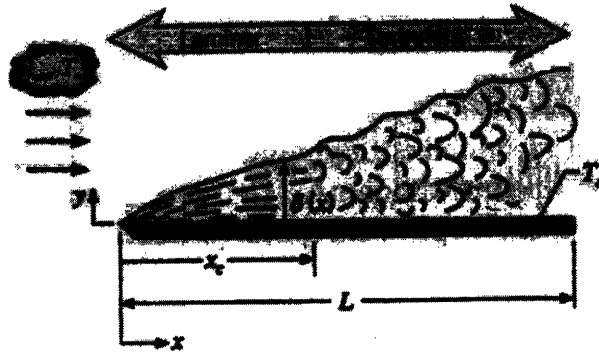


**Figure 6B. Boundary layer shift from laminar to turbulent for a flow over a stationary, semi-infinite, flat plate [59].**

Determination of flow type is done through the use of the dimensionless grouping of variables call the Reynolds number:

$$Re_x = \frac{VL}{\nu}$$

where  $V$  is the velocity of the sheet. The length,  $L$ , of the sheet was assumed to be the vertical height that the sheet travels in the furnace. Thus, each time the sheet changed directions from traveling up to down, a new semi-infinite flat plate was assumed to start. As stated before, the vertical travel in the furnace and thus the length,  $L$ , was assumed to be 8 m.

The transition from laminar to turbulent flow typically occurs at a Reynolds number between 300,000 and 500,000. Tsou, et al. [60] found that the critical Reynolds number for the laminar to turbulent transition flow transition to be substantially higher for a continuously moving plate as compared to a flow over a semi-infinite, stationary, flat plate. Therefore, this analysis assumes that heat transfer will only occur in the laminar regime.

The Nusselt number, the dimensionless temperature gradient at the surface, provides a measure of the convective heat transfer at the surface and has been found to depend on  $Re$  and  $Pr$ . Therefore, if the fluid flow over the entire surface is laminar, the average Nusselt number will be

$$Nu_x = 0.664 Re_x^{1/2} Pr^{1/3}$$

for  $Pr \geq 0.6$ . The Prandtl number,  $Pr$ , is a property of the fluid and is the ratio of the momentum and thermal diffusivities,

$$Pr = \frac{c_p \mu}{k} = \frac{\nu}{\alpha}$$

where  $c_p$  is the specific heat,  $\mu$  is the viscosity,  $k$  is the thermal conductivity,  $\nu$  is the kinematic viscosity and  $\alpha$  is the thermal diffusivity. The  $Pr$  for air remains nearly constant at  $\sim 0.7$  from 300 – 1400 K which are the expected temperatures encountered during all processing steps.

The heat transfer coefficient for convection can be determined from the Nusselt number

$$h_{c,x} = \frac{Nuk}{L}$$

and finally, from Newton's law of cooling, the rate of convection heat transfer to the plate is

$$q_{c,x} = h_{c,x}L(T_{\infty} - T_s).$$

### *B.3 Internal temperature gradient check*

The Biot number, Bi, is related to the heat transfer resistance at the surface of an object to the internal resistance to heat transfer. For  $Bi < 0.1$ , internal temperature gradients are negligible, heat transfer is controlled by the surface resistance and the Newtonian heating equation applies. Therefore,

$$Bi = \frac{(h_r + h_c)k}{L}$$

where  $h_r$  is the radiant heat transfer coefficient,  $h_c$  is the convective heat transfer coefficient, and  $L$  is the sheet thickness. Since the sum of the heat transfer coefficients is never greater than 10 and assuming a constant 304 stainless steel thermal conductivity of 21 W/m\*K and a sheet thickness of 1 mm, the Bi is approximately 0.0005 which is well under the condition for internal temperature gradients.

### *B.4 Sheet temperature change*

The time required to heat the sheet up to the necessary annealing temperature can be calculated by assuming Newtonian heating. Since the sheet is traveling at a constant velocity, the segment area was divided by the velocity to determine the appropriate fraction of heat transferred through radiation while in a particular viewing factor area. The heat transferred,  $q_r$  and  $q_c$ , through radiation and convection respectively was added and the change in temperature was calculated:

$$T_f = T_i + \frac{(q_r + q_c)}{C_p \rho A L}$$

where  $C_p$  is the specific heat (assumed to hold constant at 580 J/kg\*K),  $\rho$  is the density (assumed to hold constant at 8100 kg/m<sup>3</sup>),  $A$  is the area of the segment and  $L$  is the sheet thickness. The temperature of each 0.1 m segment was calculated for each 0.1 m of travel through the furnace. Temperature and heat transfer profiles for sheet velocities of 0.2 m/s and 1 m/s are shown in Figures 7B and 8B for a 1 mm sheet in a furnace with ~1250°C radiant tubes, a furnace atmosphere temperature of ~1000°C, and a sheet emissivity of 0.3. At 0.2 m/s, the sheet has much more radiant heat transfer as shown by the peakedness of the profile when the segment passes directly under the tubes slowly enough to absorb as significant amount of the tubes radiant heat. At 1 m/s, the sheet is moving much faster not allowing the segment to reside and pick up as much direct radiant heat from any one tube at a time. However, convective heat transfer is increased due to the increased velocity of the sheet.

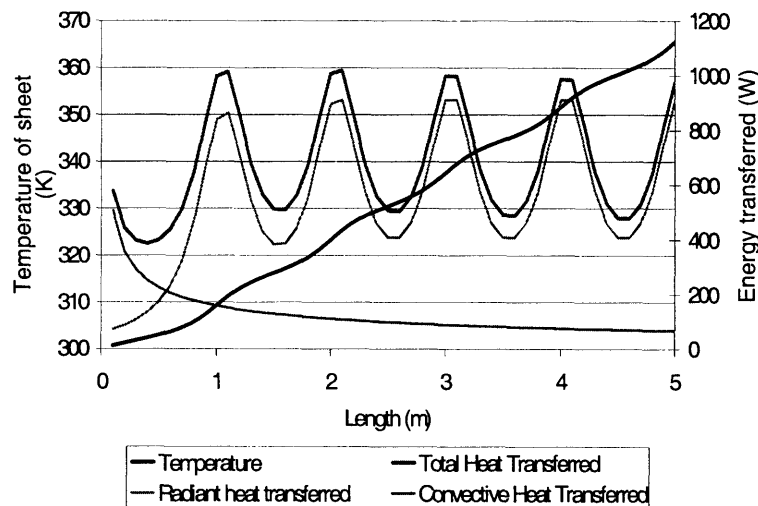


**Figure 7B. Temperature and heat transfer profiles for sheet velocities of 0.2 m/s.**

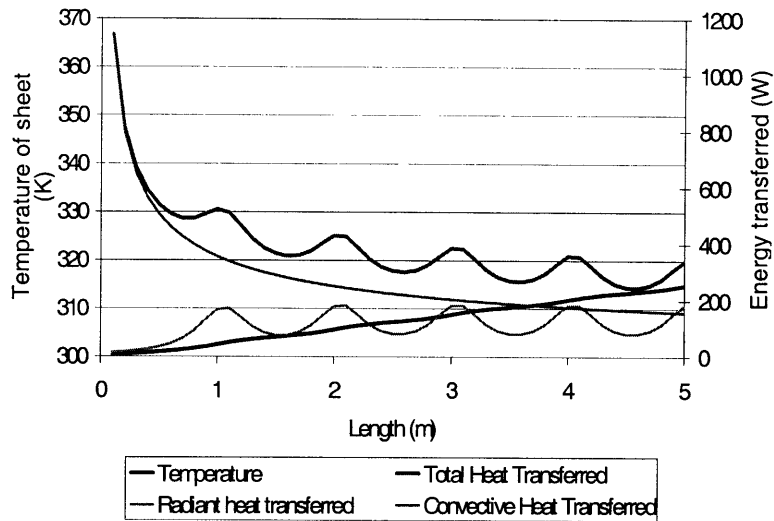


**Figure 8B. Temperature and heat transfer profiles for sheet velocities of 1 m/s.**

The time required for the sheet's temperature to increase to  $\sim 900^{\circ}\text{C}$  ( $\sim 1175\text{K}$ ) is the same regardless of heat transfer mechanism or velocity as shown in Figure 9B.

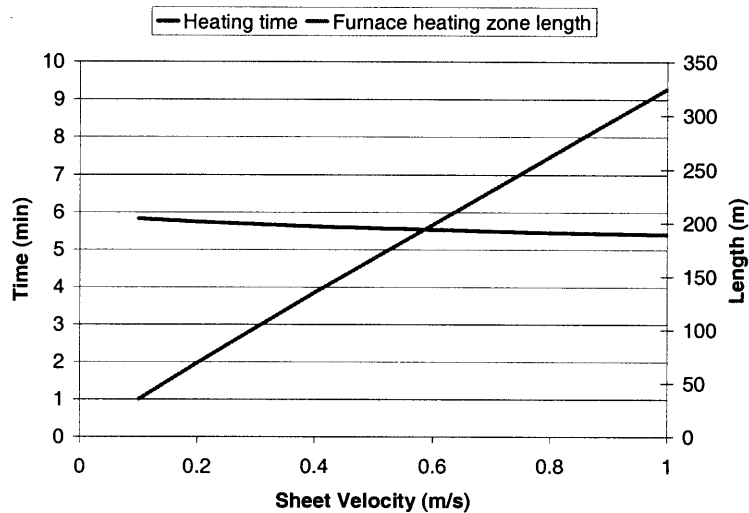


**Figure 9B. Time and length required for the sheet's temperature to increase to  $\sim 900^{\circ}\text{C}$ .**

However, the length of travel inside the furnace to attain  $\sim 900^{\circ}\text{C}$  increases linearly with the velocity. The greater length necessary at higher sheet velocities requires and larger and more expensive furnace. However, reducing the velocity reduces the possible rate of

production. This tradeoff of furnace length vs. velocity and production rate will be important to the economic analysis later.

## Appendix C: Derivation of Cooling Process Equations

Cooling of the sheet was calculated for a free jet of air impinging upon the surface of the sheet once it has exited the furnace and a schematic of this is shown in Figure 1C.

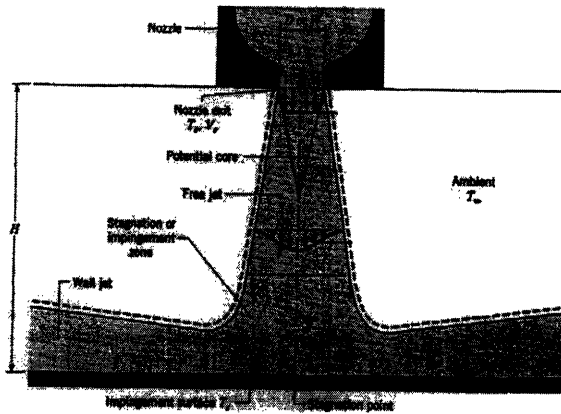


Figure 1C. Schematic of the free jet of air impinging on the surface [59].

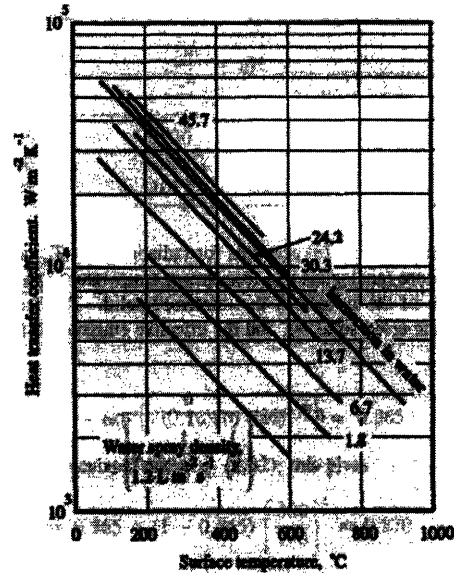


Figure 2C. Heat transfer coefficient as a function of surface temperature during spray cooling with different intensities [53].

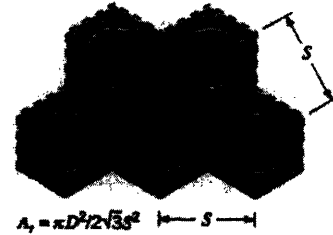
The quickest way to cool the sheet would have been to use water spray cooling where a jet of water impinges onto the hot annealed sheet with some water spray density. However, the Biot number must again be calculated to make sure that no internal temperature gradients exist. For a 1 mm sheet of type 304 stainless steel (21 W/mK), the maximum allowed heat transfer coefficient is 2000 W/m<sup>2</sup>\*K which is much lower than the heat transfer coefficients for water spray cooling shown in Figure 2C.

Therefore, free jets of air can be used to cool the sheet much in the same manner. The Nusselt number correlation for an array of round nozzles can be obtained from Incropera and DeWitt [59]:

$$\frac{\overline{Nu}}{Pr^{0.42}} = \left[ 1 + \left( \frac{H/D}{0.6/A_r^{1/2}} \right)^6 \right]^{-0.05} * 2A_r^{1/2} \frac{1 - 2.2A_r^{1/2}}{1 + 0.2(H/D - 6)A_r^{1/2}} * 0.5 Re^{2/3}$$

where H is the height of the nozzle above the sheet (1 m), D is the nozzle diameter (0.02 m), Re is the Reynolds number (velocity of 0.75 m/s and air @ 25°C) and the values assumed for the calculation are shown in parentheses. The relative nozzle area,  $A_r$ , was calculated for a staggered array of round jets as shown in Figure 3C which is calculated from:

$$A_r = \frac{\pi D^2}{2\sqrt{3}S^2}$$



where S is the distance between jets centers (0.2 m).

**Figure 3C. Staggered array of round jets [59].**

The average heat transfer coefficient can be obtained from the Nusselt number by:

$$\bar{h} = \frac{\overline{Nuk}}{D}$$

where k is the thermal conductivity of the sheet (~21W/m\*K). For the assumed values, the average heat transfer coefficient is ~1950 W/m<sup>2</sup>\*K which is just below the maximum allowed for neglect of internal temperature gradients to ensure even cooling and no thermal stresses or deformation from rapid cooling.

The sheet temperature vs. the length of continuous air jet application is shown for several velocities of a 1 mm thick sheet in Figure 4C.

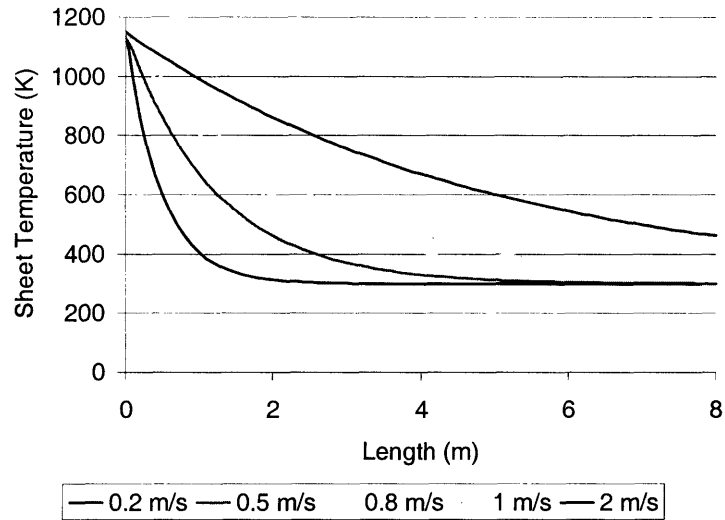


**Figure 4C. Sheet temperature vs. length of continuous air jet application for velocities of 0.2 – 2 m/s of 1 mm sheet.**

Since the sheet must be cooled to near the ambient temperature for the next cold-working iteration or final sheet coiling, an air jet array length of about between 5 – 10 meters should be used depending on the production rate of the line.